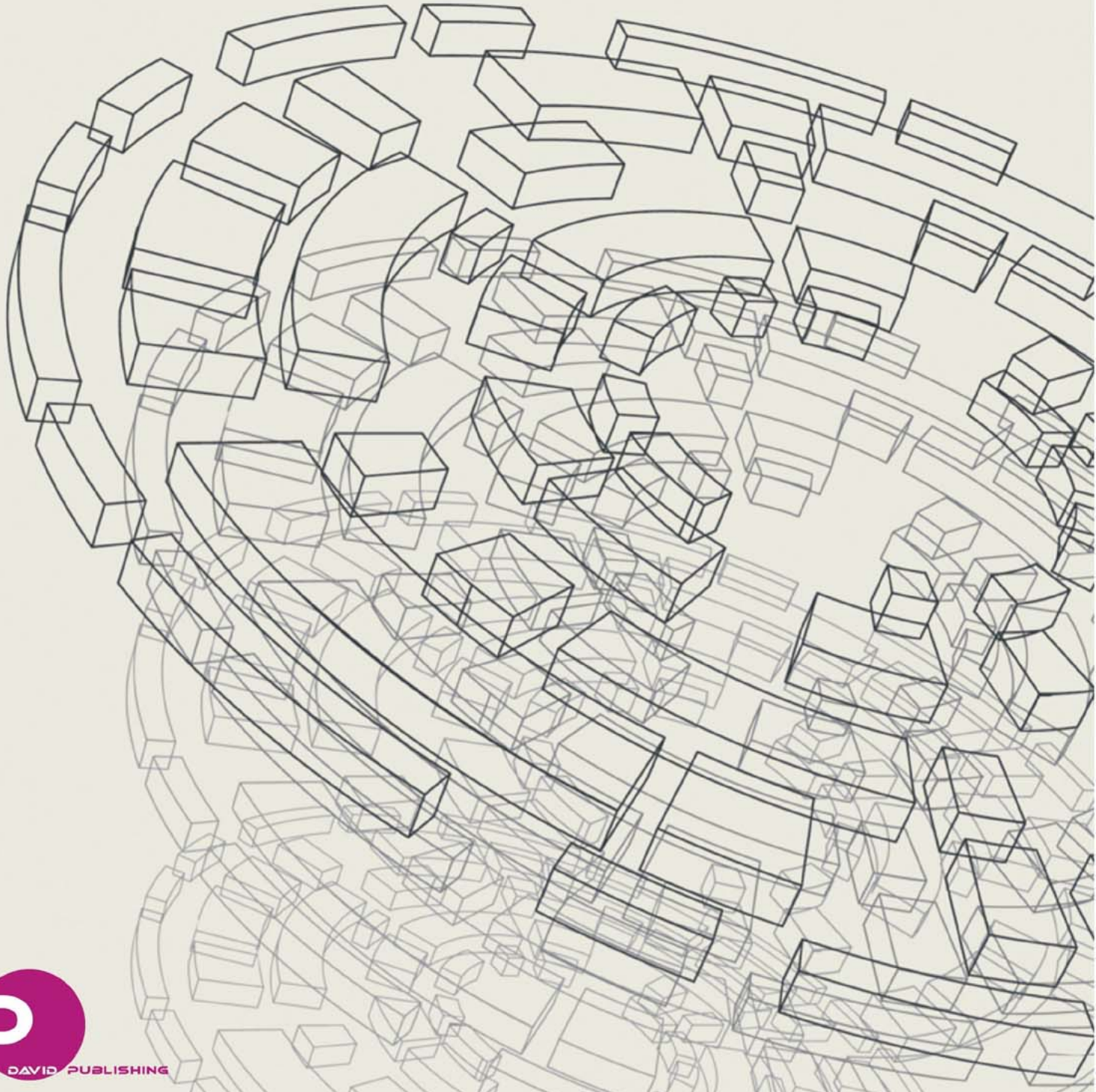

David Publishing Company

From Knowledge to Wisdom

JOURNAL OF ELECTRICAL ENGINEERING

ISSN 2328-2223
DOI:10.17265/2328-2223

Volume 7, Number 1, Jan.-Feb. 2019

Journal of Electrical Engineering

Volume 7, Number 1, Jan.-Feb. 2019 (Serial Number 26)

David Publishing Company
www.davidpublisher.com

Publication Information:
Journal of Electrical Engineering is published bimonthly in hard copy (ISSN 2328-2223) by David Publishing Company located at 616 Corporate Way, Suite 2-4876 Valley Cottage, NY 10989, USA.

Aims and Scope:
Journal of Electrical Engineering, a bimonthly professional academic journal, covers all sorts of research on electronics and microelectronics, power engineering, energy materials, signal processing, communications and networking, automatic control system, optoelectronics, bioelectrical engineering and other relevant fields.

Editorial Board Members:
Anjan Biswas (USA), Marian Apostol (Romania), Gurevich Yuri Genrijovich (Mexico), Nader Shehata (Egypt), Radian G. Belu (USA), Ivan Yukhymovych Protsenko (Ukraine), Mário Pedro Guerreiro Marques da Silva (Portugal), Vladimir A. Levchenko (Russia), Waqas Ahmed Imtiaz (Pakistan), A. Sertap Kavasoglu (Turkey), Amar Rouane (France), Joon Hoon Park (Korea), Adel Bouallegue (Tunisia), Yuri Ivanovich Choni (Russia), Sameir M. Ali Hamed (Sudan), Tran Cong Hung (Vietnam), Behrooz Shahsavari (USA), Miryala Muralidhar (Japan), Fethi CHOUBANI (Tunisia), Igor Bdikin (Portugal), Hazry Desa (Malaysia), Slava Yordanova (Bulgaria), Jimsher Aneli (Georgia), Takashiro Akitsu (Japan), Cheng Song (China), Jinsoo Song (South Korea), Ibrahim Fathy El-Said Tarrad (Egypt), Nan Wang (USA), Salvatore Magazu (Italy), Patrick VAUDON (France), Aexksi Gerasimovi (Georgia) and so on.

Manuscripts and correspondence are invited for publication. You can submit your papers via web submission, or E-mail to electrical@davidpublishing.com. Submission guidelines and web submission system are available at http://www.davidpublisher.com.

Editorial Office:
616 Corporate Way, Suite 2-4876 Valley Cottage, NY 10989, USA.
Tel: 1-323-984-7526, 323-410-1082; Fax: 1-323-984-7374, 323-908-0457.
E-mail: electrical@davidpublishing.com

Copyright©2019 by David Publishing Company and individual contributors. All rights reserved. David Publishing Company holds the exclusive copyright of all the contents of this journal. In accordance with the international convention, no part of this journal may be reproduced or transmitted by any media or publishing organs (including various websites) without the written permission of the copyright holder. Otherwise, any conduct would be considered as the violation of the copyright. The contents of this journal are available for any citation. However, all the citations should be clearly indicated with the title of this journal, serial number and the name of the author.

Abstracted/Indexed in:
Cambridge Science Abstracts (CSA)
China National Knowledge Infrastructure (CNKI)
Google Scholar
CrossRef
J-Gate
Polish Scholarly Bibliography (PBN)
Ulrich's Periodicals Directory
WorldCat

Subscription Information:
Price (per year): Print $300.

David Publishing Company
616 Corporate Way, Suite 2-4876 Valley Cottage, NY 10989, USA.
Tel: 1-323-984-7526, 323-410-1082; Fax: 1-323-984-7374, 323-908-0457.
E-mail: order@davidpublishing.com

David Publishing Company
www.davidpublisher.com

Journal of Electrical Engineering

Volume 7, Number 1, Jan.-Feb. 2019 (Serial Number 26)

Contents

Journal of Electrical Engineering 7 (2019) 1-7
doi: 10.17265/2328-2223/2019.01.001

Training of Multi-layered Neural Network for Data Enlargement Processing Using an Activity Function

Betere Job Isaac[1], Hiroshi Kinjo[2], Kunihiko Nakazono[2] and Naoki Oshiro[2]

1. Mechanical Systems Engineering Course, Graduate School of Engineering and Science, University of the Ryukyus Senbaru 1, Nishihara, Okinawa 903-0213, Japan

2. Faculty of Engineering, University of the Ryukyus Senbaru 1, Nishihara, Okinawa 903-0213, Japan

Abstract: In this paper, we present a study on activity functions for an MLNN (multi-layered neural network) and propose a suitable activity function for data enlargement processing. We have carefully studied the training performance of Sigmoid, ReLu, Leaky-ReLu and L & exp. activity functions for few inputs to multiple output training patterns. Our MLNNs model has L hidden layers with two or three inputs to four or six outputs data variations by BP (backpropagation) NN (neural network) training. We focused on the multi teacher training signals to investigate and evaluate the training performance in MLNNs to select the best and good activity function for data enlargement and hence could be applicable for image and signal processing (synaptic divergence) along with the proposed methods with convolution networks. We specifically used four activity functions from which we found out that L & exp. activity function can suite DENN (data enlargement neural network) training since it could give the highest percentage training abilities compared to the other activity functions of Sigmoid, ReLu and Leaky-ReLu during simulation and training of data in the network. And finally, we recommend L & exp. function to be good for MLNNs and may be applicable for signal processing of data and information enlargement because of its performance training characteristics with multiple teacher training patterns using original generated data and hence can be tried with CNN (convolution neural networks) of image processing.

Key words: Data enlargement processing, MLNN, activity function, multi teacher training signals, BP NN, CNN.

1. Introduction

In recent years, the application of NN (neural networks) about intelligent systems has attracted attention and lots of papers and applications have been presented. To mention a few, image processing and recognition technology in intelligent systems occupy a big percentage. It has been put to practical use in scenes where large amounts of data are handled and have been proved by many increasing numbers of researchers [1-3] especially for signal processing as to manage data transfer effectively with other systems to overcome conventional means particularly [4].

Many scientists have undergone a resurgence in computation research community from the field of NNs and deep machine learning. Furthermore, recently more research has been reported on multi hidden layer NN training [5]. Earlier scientists were motivated in large part by visions of imbuing computer programs with life-like ability to self-replicate and with adaptive capability to learn the environment in terms of artificial intelligence. The application of NNs about image processing and recognition technology in intelligent control systems indicates poor training performance of the sigmoid function due to the gradient disappearance problem with BP (backpropagation) NN training [6, 7]. It is also said that ReLu function is good compared to other activity functions in the field of 2D image processing and recognition [8]. We have also noted that Leaky-ReLu function is almost like ReLu function although with a slight improvement on the training results and can accommodate more characteristic values for BP NN training. Therefore, our motivation interest was to further investigate more by bringing

Corresponding author: Betere Job Isaac, MSc, research fields: robotics, artificial intelligent control systems and signal processing.

more activity functions into play to select one suitable for DENN (data enlargement neural network).

In this study, we extend our proposed L & exp. activity function for multi logic training patterns with multi-layered neural training networks [9, 10]. We consider it to be good for data enlargement and can truly overcome the drawbacks of sigmoid, ReLu and Leaky-ReLu functions as used in this study using original generated data sets. We hope it can be adopted and applied to CNN (convolution neural networks) in 2D image and signal processing to examine the training performance with MLNN (multi-layered neural networks) for artificial intelligent systems.

2. NN Model

NNs are typically organized in layers. Fig. 1 shows the NN model we used in this study. Layers are made up of several interconnected nodes which contain an activation function. Patterns are presented to the network via the input layer which communicates to 5 neurons and 5 hidden layers where the actual processing is done via a system of weighted connections respectively.

The hidden layers then link to an output layer and gives the result of the desired output as shown in the feedforward NN in Fig. 1, where I, J & K are number of neurons of input layer, hidden layers and output layer respectively with L hidden layers, and t_1, t_2, t_3, t_4, t_5 and t_6 as teacher training signals.

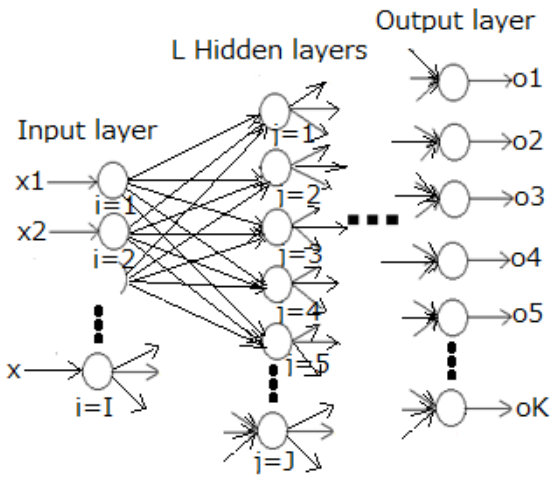

Fig. 1 MLNN.

The input/output relation of the NN is given by the following equations.

$$o_i = f^I(x_i), i = 1, 2, \dots, I \quad (1)$$

$$o_j{}^{(l)} = f^H\left(net_j{}^{(l)}\right), l = 1,2, \dots, L, j = 1, 2, \dots, J \quad (2)$$

$$net_j{}^{(l)} = \begin{cases} \sum_i w_{ji} o_i \,, l = 1 \\ \sum_j w_{jj}{}^{(l)} \, o_j{}^{(l-1)}, l \geq 2 \end{cases}$$

$$o_k = f^O(net_k), k = 1, 2, \dots, K \quad (3)$$

$$net_k = \sum_j w_{kj} \, o_j{}^{(L)}$$

where, o_i and o_j are outputs of input and hidden layers respectively, w_{ji} w_{jj} and w_{kj} are connecting weights. $f^I(.), f^H(.)$ and $f^O(.)$ are activity functions of input, hidden and output layers respectively. Many methods of NNs for signal processing have been well studied and applied for many industrial problems. There are many network types consisting of many inputs with few outputs and it is useful for image processing (CNN).

However, we consider the other type of the network construction as in Fig. 1 in respect to our motivation where the network could have multiple outputs from few inputs. This network is taken to be applicable to data enlargement fields. Simulations were basically concentrated on the functions as follows.

Sigmoid function:

$$f^H(x) = \frac{1}{1+exp^{(-x)}} \quad (4)$$

ReLu function:

$$f^H(x) = \begin{cases} x \; 0 \leq x \\ 0 \; 0 > x \end{cases} \quad (5)$$

Leaky-ReLu function:

$$f^H(x) = \begin{cases} x \; 0 \leq x \\ \alpha x \; 0 > x \end{cases} \quad (6)$$

where, α is the slope gradient of the function.

And the L & exp function as

$$f(x) = \begin{cases} x + \beta \; x \geq 0 \\ \beta \, e^x \; x < 0 \end{cases} \quad (7)$$

where, β is the intercept. This function combined both

linear part and exponential part, so we called it L & exp. function.

In this study, we have used the input and output activity function as follows:

$$f^I(x) = f^O(x) = x \tag{8}$$

3. BP for MLNN

BP training is a gradient descent algorithm. It tries to improve the performance of the neural net by reducing its error along its gradient. The error is expressed by the RMSE (root-mean-square error), which can be calculated by the error function *E* for BP as shown in the following equation.

$$\boldsymbol{E} = \frac{\mathbf{1}}{\mathbf{2}} \sum_{\boldsymbol{p=1}}^{\boldsymbol{p}} \sum_{\boldsymbol{k=1}}^{\boldsymbol{k}} \left(t_k{}^{(p)} - o_k\right)^2 \tag{9}$$

where, the error *E* is half the sum of the geometric averages of the difference between the desired output $t_k{}^{(p)}$ and the actual output o_k over all patterns p. In each training step, the weights w_{ji}, w_{jj} and w_{kj} are adjusted towards the direction of maximum decrease and scaled by some learning rate epsilon ε as shown in the following modified equation of the synaptic connection weight vector W.

$$W^{(new)} = W^{(old)} - \varepsilon \frac{\partial E}{\partial W} \tag{10}$$

The generalized delta rule of BP is applied, and the gradient is as follows with the output layer:

$$\frac{\partial E}{\partial W} = -\delta_k \, o_j{}^{(l)} \tag{11}$$

where, δ_k is as follows:

$$\delta_k = (t_k - o_k) f^o{}'(net_k) \tag{12}$$

and, for the hidden layers as follows:

$$\frac{\partial E}{\partial W} = -\delta_j{}^{(l)} o_j{}^{(l-1)} \tag{13}$$

where, $\delta_j{}^{(l)}$ is as follows:

$$\delta_j{}^{(l)} = \sum \{\delta_j{}^{(l+1)} w_{jj}{}^{(l+1)}\} f^H{}'\left(net_j{}^{(l)}\right), l = L-1, L-2, \ldots, 2, 1 \tag{14}$$

where, $f^H{}'(.)$ is the derivative of the activity function.

Derived sigmoid function:

$$f^H{}'(x) = f^H(x)(1 - f^H(x)) \tag{15}$$

Derived ReLu function as:

$$f^H{}'(x) = \begin{cases} 1 & 0 \le x \\ 0 & 0 > x \end{cases} \tag{16}$$

Derived Leaky-ReLu function:

$$f^H{}'(x) = \begin{cases} 1 & 0 \le x \\ \alpha & 0 > x \end{cases} \tag{17}$$

And the derived L & exp. function as:

$$f^H{}'(x) = \begin{cases} 1 & x \ge 0 \\ \beta \, e^x & x < 0 \end{cases} \tag{18}$$

4. Experiment Simulations

Tables 1 and 2 show the parameters we used to build the NN training model for our study. We assumed these parameters to design a simple data enlargement training network from our original generated data sets to evaluate the training performance of various activity functions in an MLNN.

Tables 3 and 4 show the training patterns. We have two sets of training patterns representing two inputs to four outputs and three inputs to six outputs for training the data in the network. In here, x_1, x_2 and x_3 are input signals used to generate teacher training signals by magnifying each input signal twice or by three signals and more (replicated) depending on the volumes of data intended to train. t_1, t_2, t_3, t_4, t_5 and t_6 are the teacher training signals for both normal data and inverted data. Normal data are taken to be an expansion

Table 1 Constant parameter of the DENNs.

No.	Parameters	Value/method
1	No. of neurons in input layer (I)	2 or 3
2	No. of neurons in hidden layer (J)	12
3	No. of hidden neuron layers (L)	1-5
4	No. of neurons in output layer (K)	4 or 6
5	Activity functions	Sigmoid ReLu Leaky-ReLu ($\alpha = 0.2$) L & exp. ($\beta = 0.2$)

Table 2 Constant parameter of the BP.

No.	Parameters	Value/method
1	Training coefficient (ε)	0.1
2	Iterations	3,000

Table 3 Training pattern for four outputs.

Normal Data

No.	Inputs		Teacher signals			
	x_1	x_2	t_1	t_2	t_3	t_4
1	0	0	0	0	0	0
2	0	1	0	0	1	1
3	1	0	1	1	0	0
4	1	1	1	1	1	1

Inverted Data

No.	Inputs		Teacher signals			
	x_1	x_2	t_1	t_2	t_3	t_4
1	0	0	1	1	1	1
2	0	1	1	1	0	0
3	1	0	0	0	1	1
4	1	1	0	0	0	0

Table 4 Training patterns for six outputs.

Normal Data

No.	Inputs			Teacher signals					
	x_1	x_2	x_3	t_1	t_2	t_3	t_4	t_5	t_6
1	0	0	0	0	0	0	0	0	0
2	0	0	1	0	0	0	0	1	1
3	0	1	0	0	0	1	1	0	0
4	1	0	1	1	1	0	0	1	1
5	1	1	0	1	1	1	1	0	0
6	1	1	1	1	1	1	1	1	1

Inverted Data

No.	Inputs			Teacher signals					
	x_1	x_2	x_3	t_1	t_2	t_3	t_4	t_5	t_6
1	0	0	0	1	1	1	1	1	1
2	0	0	1	1	1	1	1	0	0
3	0	1	0	1	1	0	0	1	1
4	1	0	1	0	0	1	1	0	0
5	1	1	0	0	0	0	0	1	1
6	1	1	1	0	0	0	0	0	0

of the original input signal twice to have an increment on data output to represent data enlargement. Inverted data are generated from the normal data by interchanging the teacher training signals and maintaining the inputs signals for both situations. We considered a simple case of DENN (data enlargement neural network) to generate the training data sets in Tables 3 and 4 basing on 0 and 1 signals as input and output respectively for our DENN model as shown by Fig. 1 in this study. It is because we believe and consider this to be the fundamental task to discuss the training performance of MLNN training without depending on data sets such that our results can easily be confirmed.

Table 5 Successive rate for four outputs [%].

Normal Data

L	1	2	3	4	5
Sigmoid	100	100	2	0	0
ReLu	100	99	100	100	98
Leaky-ReLu	100	100	100	100	100
L & exp.	100	100	100	100	100

Inverted Data

L	1	2	3	4	5
Sigmoid	100	100	4	0	0
ReLu	0	0	0	0	0
Leaky-ReLu	0	0	0	0	0
L & exp.	100	100	100	100	99

Table 6 Successive rate for six outputs [%].

Normal Data

L	1	2	3	4	5
Sigmoid	100	100	7	0	0
ReLu	100	100	99	98	21
Leaky-ReLu	100	100	100	100	99
L & exp.	100	100	100	100	92

Inverted Data

L	1	2	3	4	5
Sigmoid	100	100	22	0	0
ReLu	0	0	0	0	0
Leaky-ReLu	0	0	0	0	0
L & exp.	89	100	100	96	81

Tables 5 and 6 show the successive training rate percentages of each activity function training performance, where, *L* is the number of hidden neuron layers.

Figs. 2-5 show the training results for normal and inverted data, where, *E* on the vertical axis is the mean value error function against iterations on the horizontal axis. The successive training condition is when $E < 0.001$.

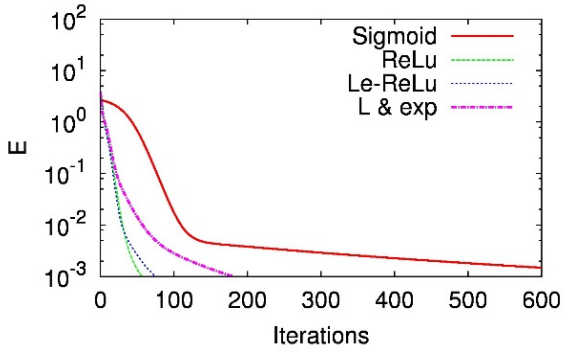

(a) $L = 1$

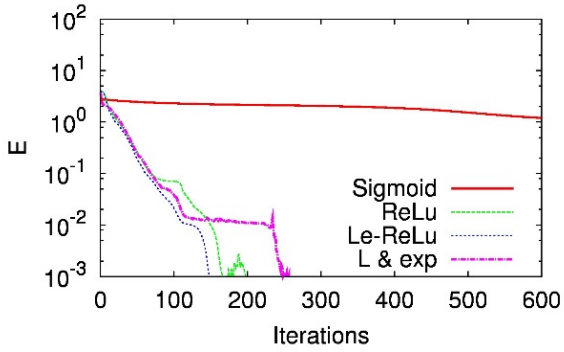

(b) $L = 3$

Fig. 2 Training results for four outputs normal data.

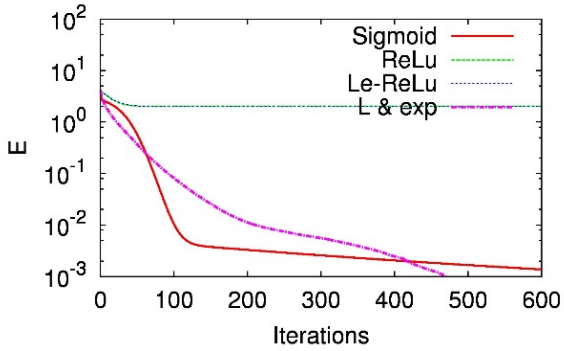

(a) $L = 1$

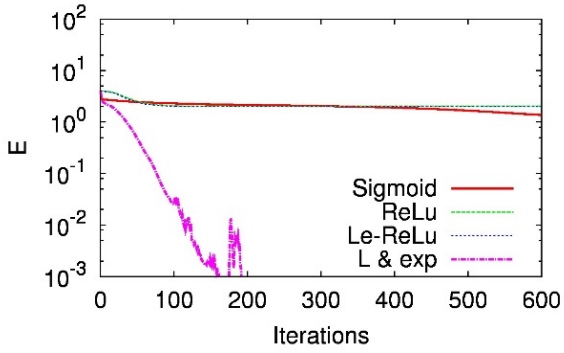

(b) $L = 3$

Fig. 3 Training results for four outputs inverted data.

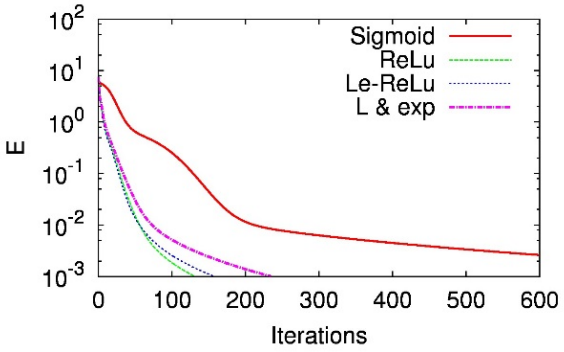

(a) $L = 1$

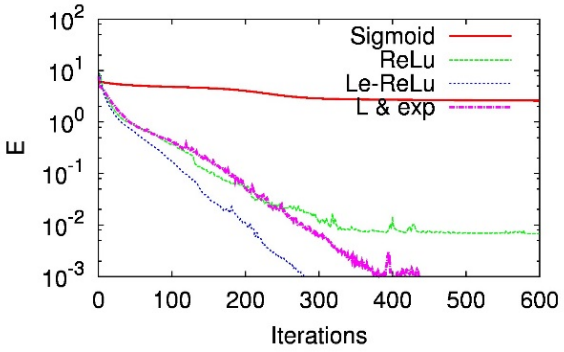

(b) $L = 3$

Fig. 4 Training results for six outputs normal data.

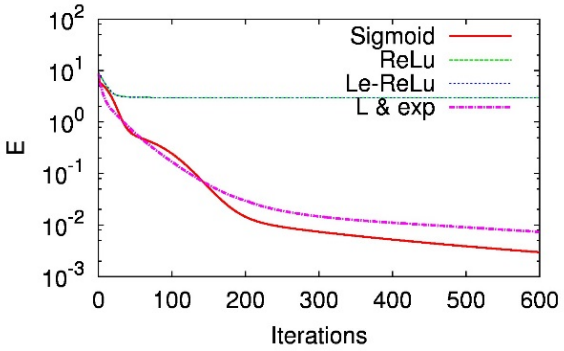

(a) $L = 1$

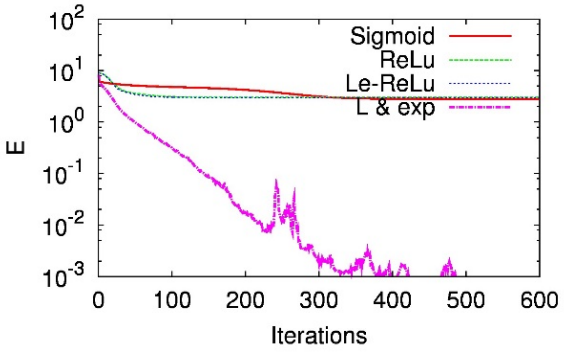

(b) $L = 3$

Fig. 5 Training results for six outputs inverted data.

5. Discussion

As per the results after training, it is seen in Tables 5 and 6 that L & exp. activity function trains all the patterns for both normal and inverted data for multi teacher training signals with the highest percentage rate in the network. Sigmoid could only train with few layers and it could appear to be good with only two layers in the network. ReLu function trained with only normal data output case and failed out when the data are inverted. Leaky-ReLu function is also seen to behave the same way since it appears to be an extended improvement of a ReLu function and seems to be good and fast during training of normal data like the ReLu function. But for wide data expression and deep training, we can see that Sigmoid, ReLu and Leaky-ReLu functions could not train satisfactorily well (Tables 5b and 6b) as L & exp. function especially when there is any change in the multi teacher training signals with many neurons and multiple layers in the network.

We considered the fact that L & exp. function is good and has an advantage over the other activity functions since it continued to satisfactorily train all patterns for both data situations without any limitation of the gradient values in the network. It can accommodate and train both positive and negative values with the increase in the number of layers and neurons in the network. It can therefore perform well with manipulated data in the any kind of system and give good results hence can be incorporated with more artificial complicated systems to handle many training parameters in any NN system and has got an advantage as compared to the other activity functions.

6. Conclusion

In this study, we investigated the training of an MLNN by an activity function for data enlargement processing. We have proved that BP training for an MLNN can give better training results using our original generated data sets as multi teacher training patterns by an activity function. In this article, few inputs to many outputs are considered to represent data enlargement where each input signal could train two teacher training signals in a four-output network. This process continued for various sets of data to confirm good training performance. We noted that L & exp. function trained all the patterns in all outputs without any interference and gave good percentage training results as compared to the other activity functions we used in the network. Thus, we propose it to be a suitable activity function to handle wide volumes of parameters in terms of data and other complicated artificial intelligence systems of CNN and machine deep learning systems. However, in this study, we have also seen that in the situation where data flows normally, ReLu and Leaky-ReLu functions are able and good to train all the patterns and very fast during training simulations, hence, can be applied to moderate data application systems. Sigmoid activity function degrades and fades out with BP especially when the numbers of layers and neurons are increased as seen for the 3rd neurons hidden layer training in the network.

For future work, we are focusing on more applications of this proposed function using the existing data sets especially in 2D image CNN and examine its training performance for image recognition and processing. We also need to find out why other activity functions like ReLu and Leaky-ReLu failed to train with MLNNs especially for data inverse training situations. Lastly, we want to examine the training performance of CNNs and MLNN in artificial intelligent systems.

References

[1] Rumelhart, D. E., McClelland, J. L., and the PDP Research group. 1986. *Parallel Distribution Processing.* MIT Press.

[2] Hassoun, M. H. 1995. *Fundamentals of Artificial Neural Networks.* MIT Press.

[3] Anderson, J. A., and Rosenfeld, R. 1988. *Neuro Computing Foundations of Research.* MIT Press.

[4] Lewis, F. L., Jagannathan, S., and Yesidirek, A. 1998. *Neural Network Control of Robot Manipulators and Nonlinear Systems*. Taylor & Francis.

[5] Kodaka, T., and Murakami, K. 2016. *Machine Learning*

and Deep Learning, Simulation by C programing, Ohmsha. (in Japanese)

[6] Okatani, T. 2015. *Deep Learning*, Kodansha. (in Japanese)

[7] Albrecht, R. F., Reeves, C. R., and Steele, N. C., eds. 1993. *Artificial Neural Nets and Genetic Algorithms*. Adolf Holzhausens Nachfolger, A-1070 Wien, Austria.

[8] Kamishima, T., Asoh, H., Yasuda, M., Maeda, S., Okanohara, D., Okatani, T., et al. *Deep Learning*. (in Japanese)

[9] Betere, J. I., Kinjo, H., et al. 2018. "Learning Performance of Linear and Exponential Activity Function with Multi-layered Neural Network." *Journal of Electrical Engineering* 6. doi: 10.17265/2328-2223/2018.03.000, USA.

[10] Betere, I. J., Kinjo, H., et al. 2018. "Investigation of Multi-layer Neural Network Performance Evolved by Genetic Algorithms." Artif Life Robotics, doi.org/10.1007/s10015-018-0494-2, Japan.

Journal of Electrical Engineering 7 (2019) 8-13
doi: 10.17265/2328-2223/2019.01.002

Development and Research of Bypass Device to Improve DC Grid Performance

Jongman Kim[1], Seokhoon Hong[2] and Beobseong Song[2]

1. Jeonnam State University, Jeonnam 57337, Republic of Korea

2. TEF Company Limited, Jeonnam 57903, Republic of Korea

Abstract: Among the factors determining the performance of the new renewable energy system, the processing part of the untreated DC power is a very important element. In fact, the area where the loss of the new renewable energy system is greatest is also the DC transmission and distribution technology. It is critical to prevent this loss and to improve the performance of the system, and analyze the performance of the resulting through the application of the resulting algorithms. In this thesis, we are discussing ways to calibrate the error in the PV distribution system within the solar power generation system using the Bypass Line Configuration Algorithm. I would like to note that if the operation of the Bypass Line device generates electrical abnormalities in the system's circuits, it can recover the performance of the system, thereby improving performance.

Key words: DC grid, bypass diode, DC transmission.

1. Introduction

Photovoltaic systems vary in performance depending on the change in environmental factors, even though installation sites, methods, power conditions, forms, etc. are the same. In order to achieve the full performance of the solar power system, it is necessary to quantify the performance characteristics including installation and installation conditions of high-performance products, and the overall performance characteristics, such as the performance estimation, and the loss of performance [3]. Improved reliability is also needed to improve the performance of the solar power generation system. All solar power stations consist of a string circuit separated by a minimum generator for each generation unit, and are generally not reliable for the over-current isolation devices inserted in each circuit. In order to improve the performance of the system problem, such as shutdown systems due to low stability, we intend to develop a joint control technology, power quality and supply stabilization system for the application of large scale systems.

Corresponding author: Jongman Kim, Ph.D., professor, research fields: renewable energy, electrical engineering.

2. Automatic Power Transfer System Control Management Unit

2.1 Proposed String Configuration System

In the case of the currently distributed systems, the contact with the load on the load cell module that is connection board is located in the center of the colony, and the power line of all the modules in the vicinity is taken in and processed. It has aspects that violate the criteria for determining whether power is normal. This can be found in terms of convenient management and risk management, which can minimize problems, which are common requirements for solar power plant operators as well as clients.

First, it should establish a system which ensures convenient construction, effective management, and minimizes risk by improving electrical stability and providing parts that meet management standards. In addition, the configuration of the solar control system must be ensured in order to maintain electrical protection of the solar power system and to maintain

the smooth electric power generation performance and electrical efficiency. In this paper, we will deal with the automatic switching system, its monitoring system and communication method for safety management when abnormal voltage is generated.

2.2 Automatic Power Conversion System Control Management

In monitoring and control system of DC power of solar power plant, system for transmission and distribution is constructed by using elements such as blocking diodes to extend system stability. In addition, the development of control devices using the power sensor module and the monitoring system using the remote communication technology are also integrated into the solar power management system in Fig. 1.

The techniques and components required for the development of stable DC power processing and transmission and distribution to be proposed in this paper are as follows.

① Constructing integrated system by combining developed element technologies;

② Configuration of current processing unit with DC collector by unit capacity;

③ Composition of communication network through wireless communication module built in DC collecting device;

④ Comprehensive data collection and processing.

In this system, the current/voltage value is measured by the sensor and input to the MCU (micro controller unit), and the comparison operation determines whether to shut off or open the circuit.

Fig. 2 is a block diagram showing the method of the automatic power conversion system.

2.3 Real Time Control Algorithm

The development of a method for increasing the stability of the power connection point of the photovoltaic system can improve the performance of the system. This system is used as a power electronic component for installation, and can be applied in the field without a procedure such as specification or certification.

In order to facilitate the configuration and management of the communication lines of the power line and the sensor module in the per-channel power processing system, a system of 30-40 kW unit is usually constructed. Fig. 3 shows the generic configuration of a real-time sequence for PV system control.

Unlike the system in Fig. 3, which is generally used, the characteristics of the proposed system are as follows.

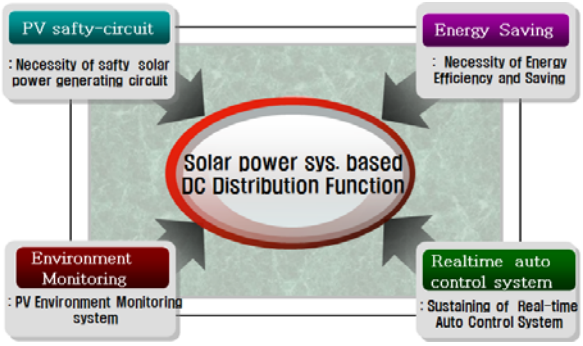

Fig. 1 The final development system of proposed solar power DC distribution system.

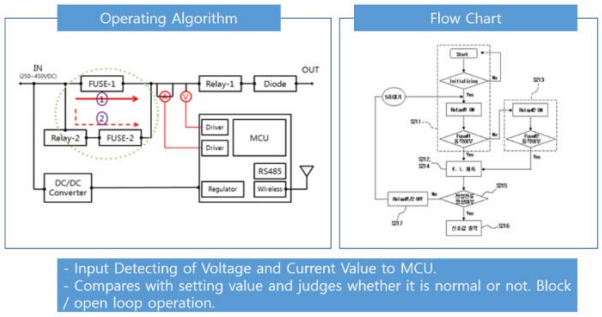

Fig. 2 Automatic power conversion system block diagram.

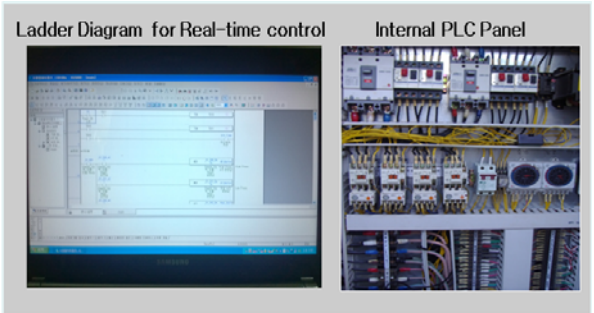

Fig. 3 Generic model of real-time sequence logic for PV system control.

The automatic power switching system has improved the stability of the system by constructing a circuit for improving the stability of the photovoltaic system. The basic line operation connecting the fuse-1 to the relay-1 to the first lane is provided as a line that is normally operated. When the power abnormality is physically detected or is detected by an abnormality of the parameter, it is switched to Relay-2 → Fuse-2 line through the operation of the automatic power switching operation circuit to correct the operation clearance according to instantaneous power change [1].

Fig. 4 shows the operating circuit in the steady state, and Fig. 5 shows the operating state of the automatic power switching system when the fault occurs.

In order to improve system performance, it is necessary to integrate the monitoring system configuration technology. Power monitoring and monitoring services are not widely available in low-capacity photovoltaic power generation facilities. This is because a large investment cost is required to construct a power management supplementary service system for a low-capacity photovoltaic power generation facility.

The application of this system is technically and economically worthy of alleviating the problem of the installation cost that has been a problem in the meantime [2].

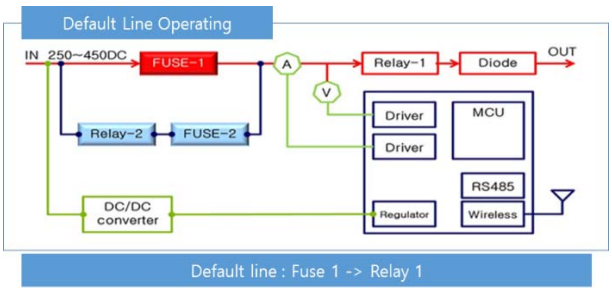

Fig. 4 Basic line operation of bypass circuit.

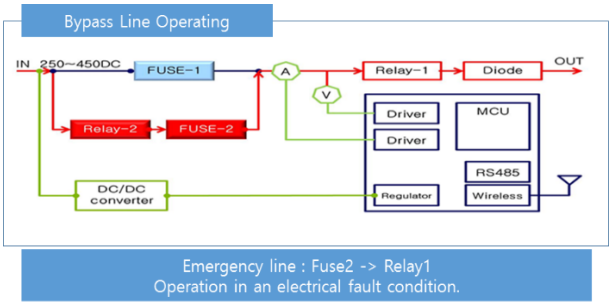

Fig. 5 Bypass line operation circuit for increasing photovoltaic power safety.

In the case of a communication system, when using a wired communication system such as RS-422 or RS-485, communication stability is good and signal fading is small, which is suitable for use in a power plant. In case of using wireless communication, it is advantageous to use 400 MHz RF method rather than WIFI or Bluetooth method for improving communication quality. Fig. 6 is the example for wireless communication system linking topology.

(1) In the case of parallel processing of data with a small amount of data (several Kbytes), there are a mode bus method and a serial data processing method which are methods used for processing a plurality of devices. However, when such a communication method causes a problem in synchronization, it seriously damages received data.

(2) The communication system designed to solve the problem distinguishes between short-distance communication and long-distance communication, and the communication load is reduced by completely separating the data acquisition unit from the data transmission/reception unit.

(3) In the case of short range communication, it acquires the analog information of the unit module and internally A/D, and transfers it to the long distance network. The data transmitted by the local area communication device having the plurality of unique IDs are inserted into the protocol of the long distance communication device and transmitted to the server.

2.4 Circuit Configuration and Design

The technic circuits and design data are required for stable DC power processing and transmission to be proposed in this paper are as follows.

Fig. 7 shows the operating circuits for SMPS (Switching Mode Power Supply) Power, MCU, Switch, LED, and Fig. 8 shows the operating circuits for Fuses and Diodes. Fig. 9 shows configuration of

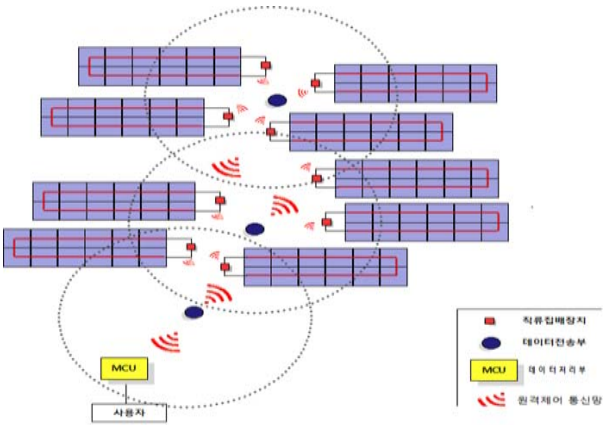

Fig. 6 DC photovoltaic power generation system.

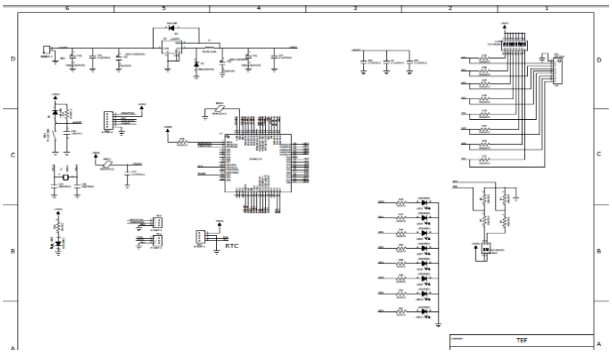

Fig. 7 Configuration of SMPS Power, MCU, Switch, LED.

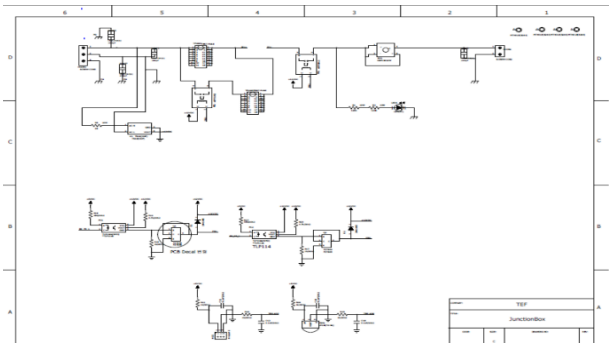

Fig. 8 Configuration of the operating circuits for Fuses and Diodes.

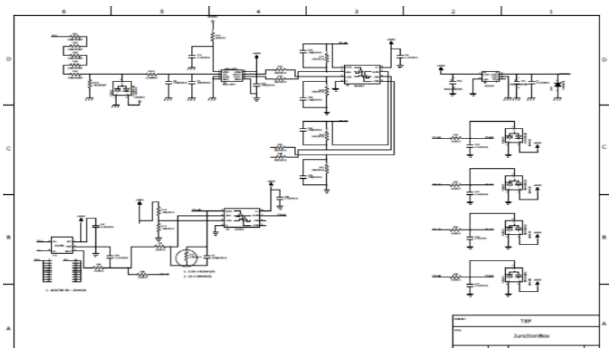

Fig. 9 Configuration of voltage-current sensing circuits.

voltage-current sensing circuits, and Fig. 10 shows configuration of wireless communication part. Fig. 11 shows configuration of artwork layout.

3. Conclusion

3.1 System Performance Test and Analysis

The circuit configuration and characteristics test of this system are as follows.

3.1.1 Stabilization Circuit of the Pickup Circuit

It is a protection circuit against spark voltage generated when PV open voltage or PV abnormality is set to 2~3 times of open voltage.

3.1.2 Breaking Current Measurement Test

The blocking/automatic power switching function is activated at the proper current, and it is possible to realize the stable bypass function. Results of breaking current measurement test are in Fig.12 as follows.

3.1.3 System Performance Analysis

(1) The SNR (signal-to-noise ratio) of the system is

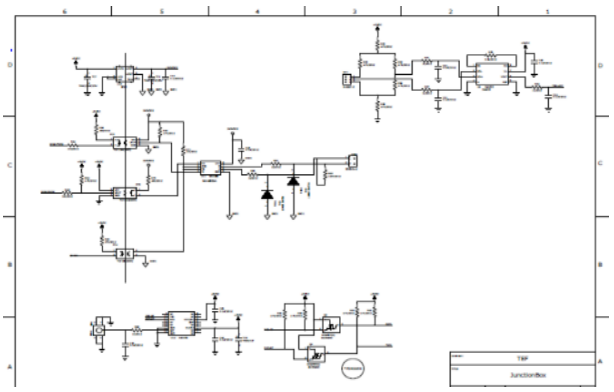

Fig. 10 Configuration of wireless communication part.

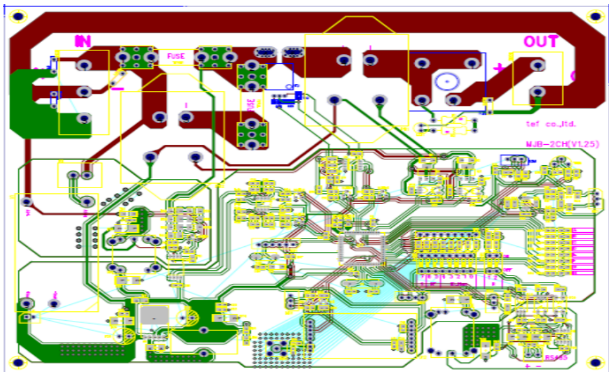

Fig. 11 Configuration of artwork layout.

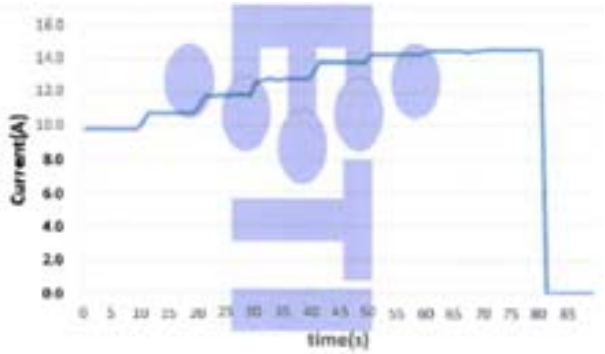

Fig. 12 Results of breaking current measurement tests.

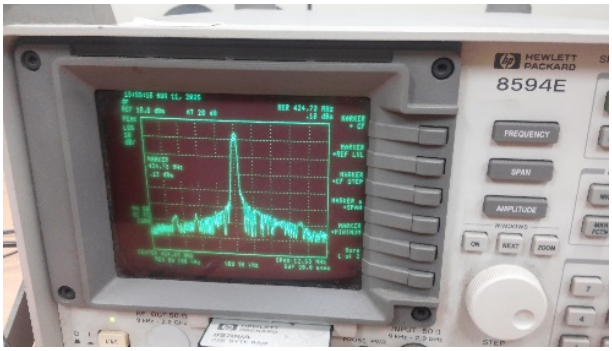

(a) SNR (more than -20 dB)

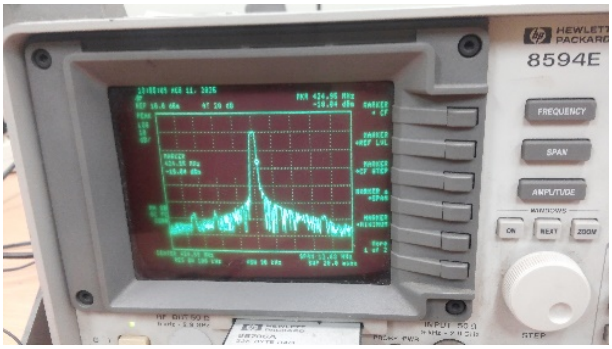

(b) SNR (more than -50 dB)

Fig. 13 Results of system performance analysis.

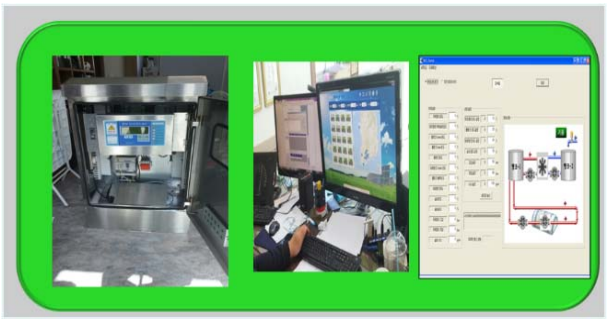

Fig. 14 System test and monitoring system configuration.

more than -20 dB and shows excellent performance in Fig. 13.

(2) The SNR of the noise region was found at more than -50 dB, and the transmission quality compared to the noise band of the signal was found to be no problem to apply to the field.

3.2 Configuration of Management System

A real-time monitoring system was constructed for monitoring and managing the system in Fig. 14.

3.3 Conclusion

In case of solar system voltage fuse failure, it is possible to monitor the overvoltage and overcurrent through the function of changing to auxiliary fuse through power relay, so that the automatic shutoff function can be confirmed when an abnormality occurs in the line.

The system has a characteristic of determining whether the line is basically opened or closed and actively judging whether the line is momentarily maintained or blocked by sensing a change in the state of the input power.

In addition, it is confirmed that real-time management of characteristics with channel compensation and emergency shutdown function is possible by constructing a real-time monitoring system for control for monitoring and managing the system.

We propose a wireless communication method of communication method used in PV power plant and through this, performance verification is accomplished. This system is an important research/development for the maintenance of the photovoltaic system and it is considered that the value of the additional research will be high in the future.

Acknowledgement

This work was supported by the Industry-University Fusion Center, under the establishing of Development of DC Power Distributed Device for DC grid Power Infrastructure.

References

[1] Kim, S. T., Park, C. H., Kang, G. H., Waithiru, C. K.,

Lawrence, H. K., Ahn, G. J., et al. 2007. "Operation Characteristics of Bypass Diode for PV Module." *Journal of KIEEME* 21 (1): 12.

[2] Gratzel, M. 2000. "Perspectives for Dye-Sensitized Nonocrystalline Solar Cells." *Prog. Photovoltaics Res. Appl.* 8: 171.

[3] Kaminski, A., Vandelle, B., Fave, A., Boyeaux, J. P., Nam, L. Q., Monna, R., et al. 2002. "Aluminium BSF in Silicon Solar Cells." *Solar Energy Material & Solar Cells* 72 (1-4): 373-9.

Journal of Electrical Engineering 7 (2019) 14-18
doi: 10.17265/2328-2223/2019.01.003

Challenges in Power Production Investment in Vietnam

Nam Hoai Nguyen, Binh Van Doan, Quyen Le Luu and Thanh Cao Nguyen

Institute of Energy Science, Vietnam Academy of Science and Technology, 18 Hoang Quoc Viet, Cau Giay, Hanoi 10072, Vietnam

Abstract: This paper presents the results of the survey to initially assess the current situation of power supply chain development in Vietnam. The research team used questionnaires to identify challenges and barriers in power production investment. Surveyors came from power generation units, power transmission and distribution units, service providers for power plants, consulting agency and research institutes. The results indicated that there is a difference among enterprises' barriers and difficulties in the management, finance and investment environment. This difference is related to the business profiles of the enterprise, its segment of the electricity generation market, capacity and experience in the market.

Key words: Power production, investment, Vietnam, policy recommendation.

1. Introduction

1.1 General

The electric power market plays an important role in power sector development of Vietnam. One of the key objectives set out for the development of Vietnamese electric power market is attracting investment from all economic sectors and gradually removing the State investment into the power industry. The electric power market has achieved positive results in terms of the performance capacity, the reliability of the system, basically power supply and demand balance. Besides, the performance of a competitive electric power market has increased the transparency and fairness in mobilizing other resources for power generation. However, there still existed certain restrictions in the market development such as subsidization; difficulty in attracting investment from foreign and private developer, efficiency of the power sector's business activities, the pressure in power price increase and the rights of customers [1, 2]. One of the primary causes is the ineffectiveness of investment attraction into the electric power market.

The authors have conducted surveys and interviewed enterprises involved in the field of electricity production in Vietnam to identify the challenges and barriers that these businesses encounter during their investment process in Vietnam. The results of the survey will contribute to the policy recommendation to ease the difficulty and promote private investment in electricity production in Vietnam in the coming time.

1.2 Overview of Power Supply Chain

Power supply chain consists of four segments: production, transmission, distribution and retail. In the production segment, the electric power is generated by the process of converting energy from hydroelectric sources, thermal energy, wind energy, geothermal or solar. The power generation is closely related to the primary energy sources such as coal, oil, gas, wind, solar and hydro resources. After being produced at the facility, the power was immediately transported to the customers through the network of transmission and distribution system. The power consuming sectors compose of agriculture-forestry-fishery, construction-industry, commerce-service, residential, and other facilities. Fig. 1 presents the power supply chain of Vietnam power industry.

Power can only be temporarily stored. The cost for storing power in the energy storage system is expensive, therefore, it should be produced at the time and amount

Corresponding author: Quyen Le Luu, MSc, research field: sustainable energy development.

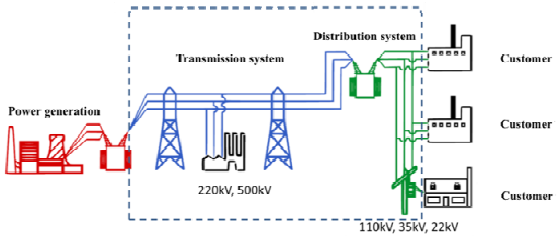

Fig. 1 Power supply chain of Vietnam power industry.

to be suitable to the demand. During the operation of the electric power system, it is compulsory that the production and consumption of electric power are simultaneous and must be always balanced. This is also the fundamental characteristics of the electric power industry which make it totally different from other sectors. If there is any potential of supply-demand imbalance due to supply or demand fluctuations, the power system operator has to apply a special mechanism to ensure that the supply is immediately balanced with the demand.

1.3 Development of Power Supply

The power market is operated and developed in accordance to objective principles such as supply and demand laws, competition rules, pricing rules, etc. Besides, the power market has a specific mechanism with several conditions for transactions between buyers and sellers to assure that supply and demand are technically balanced at all times. To meet the above conditions, technical infrastructure for the power market also has unique mechanism, structure and characteristics.

The power market development is the process to improve different components that make the market more completed. This is a synchronous and sustainable development of the basic elements of the market including supply, demand, transmission and distribution infrastructure, trading platforms and mechanisms, and electricity prices. Therefore, unlike most other products, the demand for electricity that grows too fast or is likely to outstrip supply will have a negative impact on the security of the entire power system. This difference needs to be taken into account when studying the power market development.

Power supply and demand is required to be balanced at all times. In case there is an imbalance between the power supply and demand, the power quality of the entire power system will be affected. The demand for electricity must always be fully and instantly met. The higher the consumption, the greater the capacity of production, transmission and distribution, which entails a large capital investment to build more power plants and expand the transmission and distribution infrastructure [3].

It usually takes 5 to 10 years to construct power supply or power transmission and distribution units. The construction of power related projects requires a large investment capital, up hundreds million or billions of USD. Thus, in order to ensure the stable operation of the national and provincial electricity systems with high reliability, the power development plan must always be designed for long term, usually 5 to 10 years or more. In Vietnam, this is the period for the national, provincial or municipal power development plans [3].

2. Methods

The research was done in the form of a survey using multiple-choice questionnaires and some open questions. It was conducted from June to August 2017. The survey form was sent to the surveyors through emails. The number of obtained feedback is 24, including 20 complete responses and 4 incomplete responses. Affiliations of surveyors are presented in Table 1.

Most of the survey participants are representatives of the business that have been investing into the power

Table 1 Affiliation of surveyors.

Affiliation	Number of surveyors
BOT or IPP power generation businesses	13
Researchers	6
EVN related power generation businesses	2
Transmission businesses or retailers	2
Service providers for power plants	1

sector. Some businesses also provide the transmission and distribution services. There are 17 surveyors being developers of solar power projects, wind power projects or both solar and wind power projects. Three surveyors worked for hydropower production businesses, one surveyor worked for biomass power business, and three surveyors worked for businesses operating the coal thermal power.

The survey was designed with several structured questions, used to collect testimonials of people about issues related to difficulties (internal factors) and barriers (external factors) which impact the investment and management of power generation facilities, including renewable energy.

The assessment scale is divided into 5 levels from 1 to 5. The scale of 1 is perspective to "not difficult" (or "not a barrier") for the business. Vice versa, the scale of 5 means it is "dramatically difficult" (or "significant barrier") for the business.

The authors have designed some open questions to gather the opinions of the surveyors about the macro factors such as business environment, institutional and policy framework, and electric power market. The obtained results played a key part in reviewing the proposed solutions to power market development.

3. Results

The survey results showed that the investment into electric power production has encountered the following major obstacles and difficulties, including (i) fuel supply arrangement, (ii) requirements of investment procedures, (iii) completion of construction and grid connection, (iv) arranging investment capital, (v) off-taker and (vi) difficulties from the business environment. These difficulties and barriers are structured into three main groups: difficulties and barriers in management, technique and technology; financial difficulties and barriers; and difficulties and barriers in trading environment in electricity market.

The difference among the barriers and difficulties of enterprises origins from the activities and their involvement in the market. This difference is related to the origin and composition of economic enterprises, power production market segment where they join, ability, qualifications and experience to join the market.

3.1 Management, Technique and Technology

Most of the surveyed enterprises found difficulties and barriers in fuel supply arrangement, requirement of investment procedures, completion of construction and grid connection.

Nine to twenty (9-20) surveyed businesses have noticed the difficulties and barriers in arranging material for the operation of the power plant. The barrier of material/fuel arrangement was reported by developers of coal fired power plants and biomass based thermal power plants. Meanwhile, enterprises who invested in hydropower, wind power and solar power expressed that they have many advantages when arranging fuel/source of raw material for the operation of power plants.

The investment procedures (applying for investment certificates, supplementing projects into the power development plan, setting up investment projects, reviewing the environmental impact assessment report, applying for construction permit, and license to operate the power plan, etc.) were the major hurdle for most businesses in the industry, either private enterprises, State enterprises, foreign enterprises or EVN-related enterprises. Fig. 2 presents the perception of enterprises on barrier investment procedures on the scale from 1 to 5.

The process of completing the construction, grid connection, and management and operation of the power

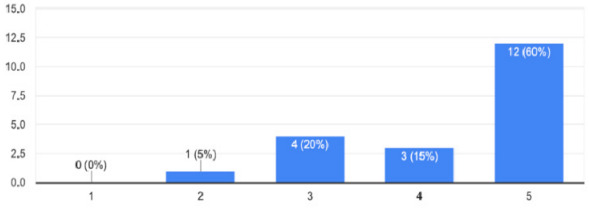

Fig. 2 Barrier on investment procedures.

plant also caused many difficulties for the business. Thirteen to twenty (13-20) business surveyed who had difficulty in this process (at the scale of 4 and 5), are private enterprises working on renewable power. The few remaining businesses with close connection to EVN or State enterprises have experienced in this process and did not treat this as a barrier. Fig. 3 indicates the difficulty of enterprises during construction completion and grid connection.

3.2 Economics and Finance

The majority of surveyed enterprises found difficulties in accessing and mobilizing investment capital for project development; and negotiating and signing contracts/agreements to purchase electricity. Fourteen (14) enterprises encountered significant barriers when approaching and mobilizing investment capital for development of power projects. No enterprises believed that they can smoothly mobilize capital. Only foreign investors and three domestic private investors found it is not significant barrier for them to arrange finance and capital for project development. The perception of capital mobilization difficulty is presented in Fig. 4.

Eighteen to twenty (18-20) surveyed enterprises considered the negotiation and signing of the power purchase agreement as an average-to-big hurdle (scale from 2 to 5), except for two EVN connected enterprises (scale 1). Enterprises, especially private enterprises encounter many difficulties in building and maintaining a team of technical staff, manage the operation of the power plant capacity and qualify to meet the requirements. With the high growth of the electricity production and supply chain in the coming time, the establishment and development of a standard technical team are forecasted to remain great difficulties for businesses who desire to invest in the production of electricity.

3.3 Business and Investment Environment

Several businesses (9 out of 20) have identified business environment in the power generation is not favorable, not to ensure the transparency in the procedures and investment procedures, licensing. Only a handful of businesses think that the procedures for conducting transactions in the power market are favorable for businesses. Eighteen to twenty (18-20) surveyed businesses expressed that the current policies for managing and operating the electric power market are incomplete. In order to enhance the investment environment in Vietnam, power developers express that there should be supportive mechanism, complete guidelines and regulations. It is also difficult for investors to access the information on policies and power development plans at all levels. The restructure of the power sector and development of the competitive power market has not shown any noticeable results, influencing the investment activities. Besides, it is not really fair for developers who are not connected to EVN to invest into power generation. Businesses' perception of difficulties in investment environment is indicated in Fig. 6.

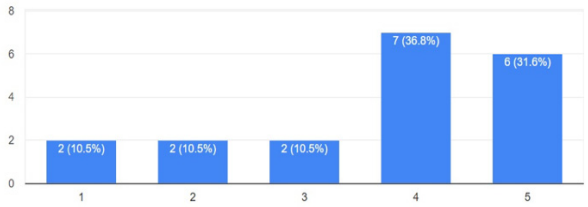

Fig. 3 Difficulty during construction completion and grid connection.

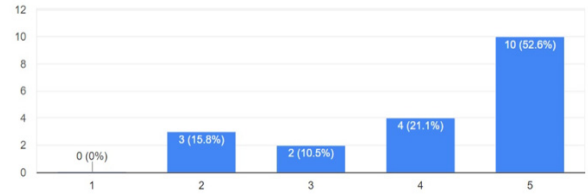

Fig. 4 Difficulty in mobilizing capital.

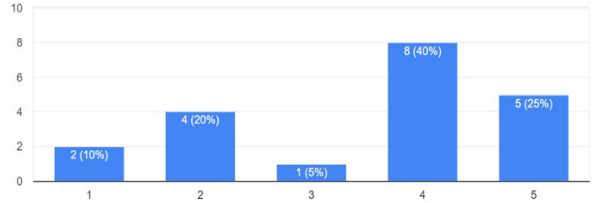

Fig. 5 Difficulty in signing the power purchase agreement.

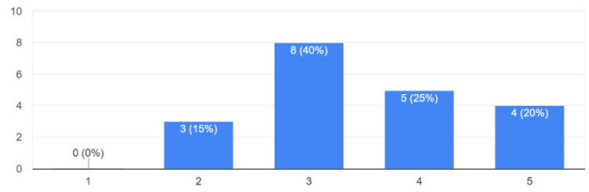

Fig. 6 Assessment of invesment environment.

4. Conclusion

The surveyed results indicated that power developers in Vietnam have been facing with several difficulties and barriers during their business investment, deployment and market entry. These difficulties include, but not limited in (i) fuel supply arrangement, (ii) requirements of investment procedures, (iii) completion of construction and grid connection; (iv) arranging investment capital, (v) off-taker and (vi) difficulties from the business environment.

There is a difference between enterprises in perception of barriers and difficulties during their activities and participation in the market. This difference is related to the origin and economic composition of the enterprises, their segment of the electricity generation market, capacity, and experience in the market. EVN related generation companies tend to face difficulties in mobilizing capital. These enterprises also showed good experience and capacity in implementing such procedures as grid connection, operation management, human resource development and negotiation and implementation of power purchase agreements. On the contrary, these are difficult challenges for private sector enterprises. Among the private companies that invest in the electricity generation market, foreign firms have a good capacity in terms of financial capacity, capital mobilization and project management. Surveyed domestic private firms showed that they still face many difficulties to improve their capacity and gain their experience in the studied issues.

In order to attract investment into the Vietnamese power production market, there are some points to be considered, including:

- Further improve the legal and policy framework and reform the administrative procedures to attract investment, especially investment in production infrastructure and electricity grid;
- Enhance the competition, ensure the fairness and transparency in the electric power trading activities and in operation of the electric power market.
- Improve the accessibility to information on planning, investment, license approval procedures for all investors and developers;
- Build capacity and train the high-quality human resources for operating the power trading platform; for construction, operation and maintenance of the power plants and other electric power works, especially renewable power projects.

References

[1] ERAV. 2015. “The Project of Detailed Designing the Competitive Wholesale Power Market of Vietnam.” Ministry of Industry and Trade, Hanoi.

[2] ERAV. 2017. *Final Report of Operating the Competitive Power Generation and Wholesale Power Market in the Pilot Period from 01 July 2016 to 30 June 2017*. ERAV.

[3] Hiep, D. X. 2012. “Establishment and Development of Power Market in Vietnam.” The State research project, Ministry of Science and Technology, Hanoi.

Journal of Electrical Engineering 7 (2019) 19-22
doi: 10.17265/2328-2223/2019.01.004

Versatile DVCC-Based Current-Mode IAFs without Parasitic Effects

Takao Tsukutani[1] and Noboru Yabuki[2]

1 National Institute of Technology, Matsue College, Matsue 690-8518, Japan

2 National Institute of Technology, Tsuyama College, Tsuyama 708-8509, Japan

Abstract: This paper introduces current-mode IAFs (inverse active filters) employing DVCCs (differential voltage current conveyors) and grounded passive elements without the parasitic effects. The IAFs enable ILP (inverse low-pass), IBP (inverse band-pass) and IHP (inverse high-pass) responses by adding the circuit current outputs suitably. Additionally the circuit parameters ω_0 and Q can be set orthogonally adjusting the circuit passive elements. An achievement example is given together with simulation results by PSPICE.

Key words: Analog circuits, IAFs, DVCCs.

1. Introduction

Active circuit with high performance has received significant attention. Numerous circuit designs employing active devices such as CCIIs (second generation current conveyors), the DVCCs and so on have been discussed in the literature earlier [1, 2].

An IAF (inverse active filter) has been used to improve the characteristic deterioration in the signal transmission, and applied to the controller in some control systems, etc. Several IAFs with active devices such as FTFNs (four-terminal floating nullors), CFOAs (current feedback operational amplifiers) and the CCIIs have been reported in the past [3-6]. The IAFs [3-5] with the FTFNs and CFOAs used ungrounded passive elements on the device's properties. Moreover a study [6] reported an IBP (inverse band-pass) filter employing the CCIIs. The IAF used the grounded passive elements, and is applied to a PID controller. However as the x-terminal of the CCII is loaded by a capacitor, consequently it leads to improper circuit performance owing to the effect of parasitic resistance at high frequency region. The CCII-based and DVCC-based IAFs considering the parasitic effects have not been yet studied sufficiently.

This paper introduces three current-mode IAFs employing the DVCCs and grounded passive elements with the mentioned points above. In the IAFs, all the x-terminals of the DVCCs are grounded through the external resistors considering the parasitic resistors. The filter circuits enable ILP, IBP and IHP responses by suitably adding the circuit current outputs. Additionally the circuit parameters ω_0 and Q can be set orthogonally according to the circuit passive elements. The voltage-mode IAFs are also presented using basic current-mode ones.

An achievement example is given with PSPICE simulation, and the circuit workability is confirmed.

2. DVCC

The symbol of the DVCC is given in Fig. 1, and hereinto it shows dual current output DVCC. The DVCC [2] with MOS transistors is shown in Fig. 2.

The standard DVCC can be characterized by the following terminal equations:

$$V_x = V_{y1} - V_{y2} - I_x R_x, \quad I_z = \pm I_x \tag{1}$$

where R_x shows the parasitic resistance at x-terminal,

Corresponding author: Takao Tsukutani, PhD, research field: analog signal processing.

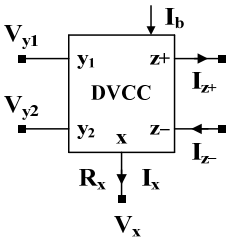

Fig. 1 Symbol for DVCC.

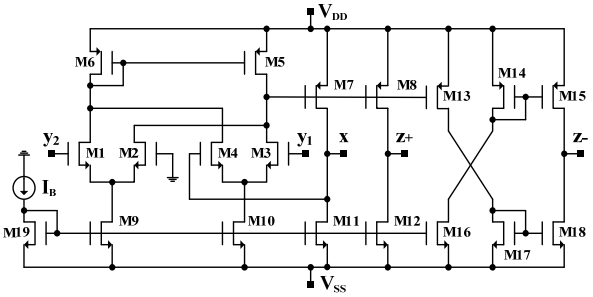

Fig. 2 DVCC with MOS transistors.

and the sign ± denotes the polarity of the current output I_z at the z-terminal.

3. IAFs and their Performances

Fig. 3 shows basic current-mode IAF circuit configurations. The IAFs are consisted of the DVCCs and grounded passive elements. In these circuits, all the x-terminals of the DVCCs are connected to the grounded resistors considering the parasitic resistances. The filter circuits in Fig. 3 can perform the ILP, IBP and IHP responses by the current addition of $I_{out}(s) = I_1(s) + I_3(s) + I_4(s)$.

Fig. 4 shows general current-mode IAF configurations employing the basic current-mode circuit above. The current output $I_{out}(s)$ is same as the basic current-mode one in Fig. 3.

The circuit transfer functions $T_{ILP}(s)$ (=$I_{out}(s)/I_{in}(s)$), $T_{IBP}(s)$ and $T_{IHP}(s)$ are given by:

$$T_{ILP}(s) = \frac{R_a}{R_b}\frac{s^2 + (1/C_1R_3)s + 1/C_1C_2R_2R_4}{1/C_1C_2R_2R_4} \quad (2)$$

$$T_{IBP}(s) = \frac{R_a}{R_b}\frac{s^2 + (1/C_1R_3)s + 1/C_1C_2R_2R_4}{(1/C_1R_3)s} \quad (3)$$

$$T_{IHP}(s) = \frac{R_a}{R_b}\frac{s^2 + (1/C_1R_3)s + 1/C_1C_2R_2R_4}{s^2} \quad (4)$$

The circuit parameters ω_0 and Q are represented as below, respectively:

$$\omega_0 = \sqrt{\frac{1}{C_1C_2R_2R_4}}, \quad Q = R_3\sqrt{\frac{C_1}{C_2R_2R_4}} \quad (5)$$

The gain constants H_{ILP}, H_{IBP} and H_{IHP} are given as:

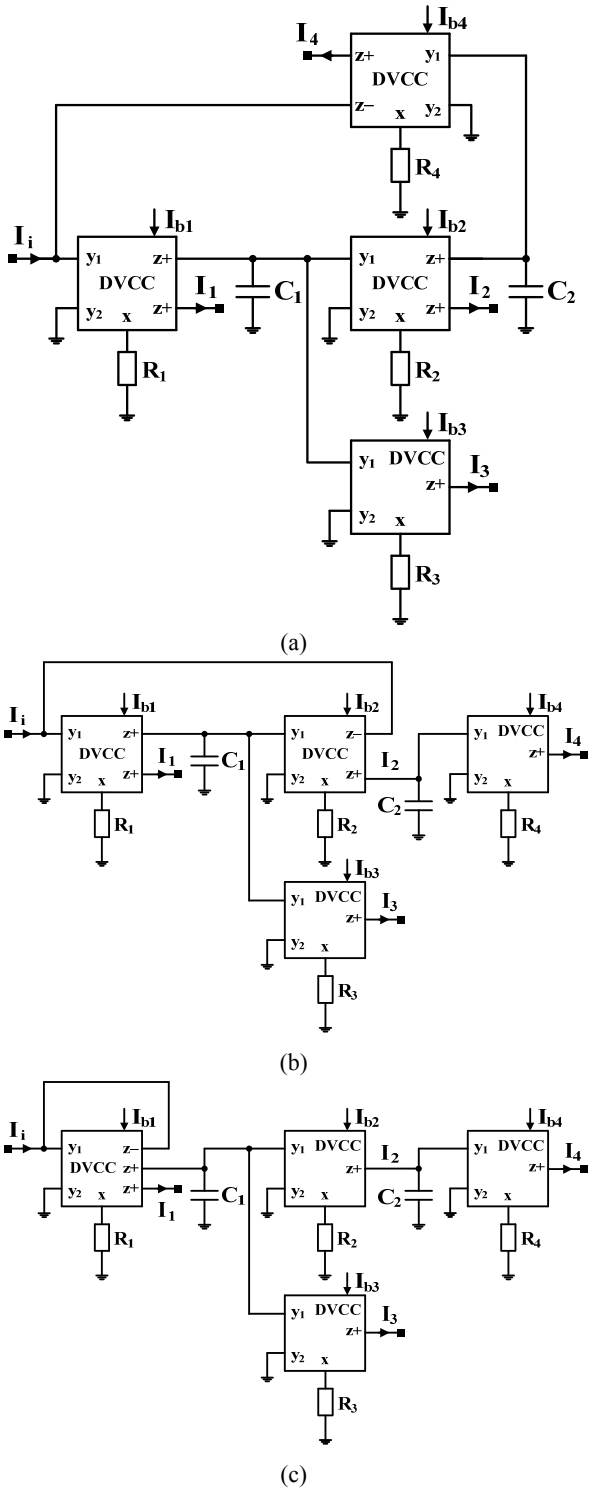

Fig. 3 Basic current-mode IAF configurations.

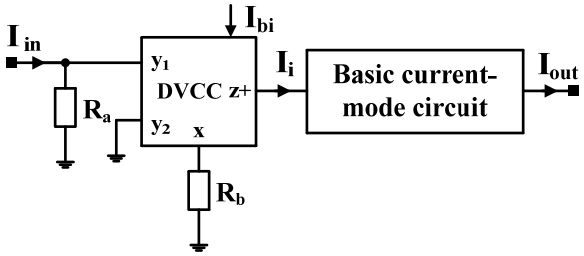

Fig. 4 General current-mode IAFs.

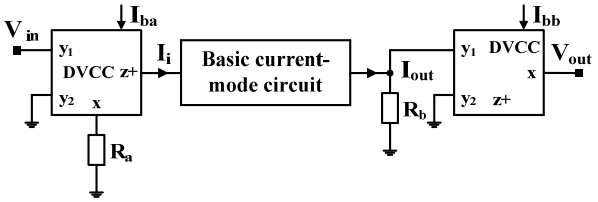

Fig. 5 Voltage-mode IAFs.

$$H_{ILP}=\frac{R_b}{R_a},\quad H_{IBP}=\frac{R_bR_3}{R_aR_2},\quad H_{IHP}=\frac{R_b}{R_a} \qquad (6)$$

Thus, the ILP, IBP and IHP responses can be achieved by simple current addition only. Moreover Eqs. (5) and (6) show the circuit parameters ω_0, Q can be set orthogonally, and the gain constants H_{ILP}, H_{IBP}, H_{IHP} are set independently.

The voltage-mode IAFs are consisted of the basic current-mode ones shown in Fig. 5. Here the voltage output $V_{out}(s)$ is obtained by converting the current output I_{out} of the basic current-mode circuit to voltage.

The circuit parameters ω_0, Q are same as the current-mode ones, meanwhile the gain constants are given as $H_{ILP}=R_a/R_b$; $H_{IBP}=R_3R_a/R_2R_b$; and $H_{IHP}=R_a/R_b$, respectively.

4. A Design Example and Simulation Results

In order to verify our proposal, we tried to realize current-mode ILP and IBP responses using PSPICE simulation program. As a design example, we consider a specification with $f_0(=\omega_0/2\pi)$ = 500 kHz, Q = 1.0 and H_{ILP} = H_{IBP} = 1.0. In the simulation, we have used a macro model of the DVCC shown in Fig. 2.

In accordance with the specification above, we have set the circuit resistors R_i, capacitors C_i and bias currents I_b listed in Table 1. Additionally the input current and power supply voltage were set at I_{in} = 10 μA and V_{DD} = -V_{SS} = 0.8 V, respectively.

Fig. 6 shows the simulated ILP and IBP responses. The marks show the simulation responses, meanwhile the solid lines are the theoretical ones. We can find that the simulation responses are favorable enough over a wide range of frequencies. In these circuits, the power dissipations were 0.383 mW and 1.22 mW, respectively.

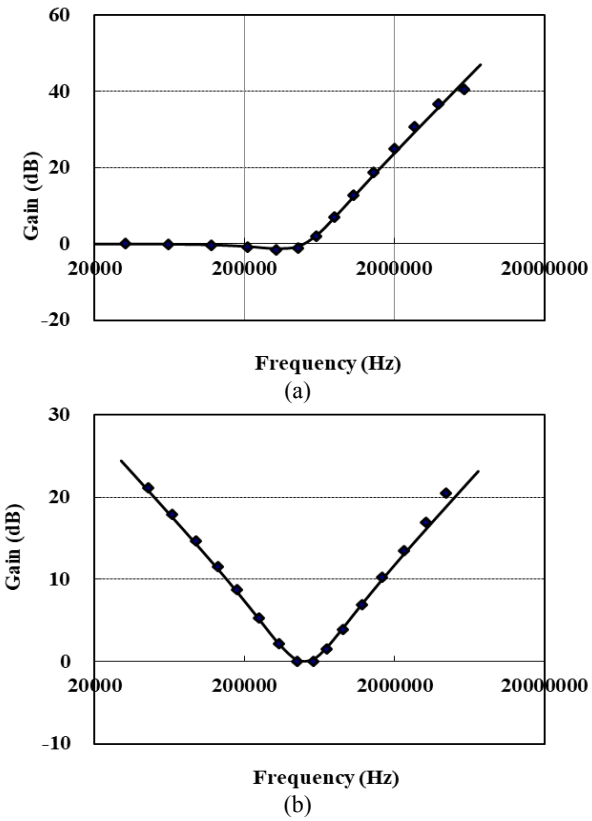

Fig. 6 Simulation responses.

Table 1 Circuit element values.

x	ILP	IBP
R_1	0.1 kΩ	20 kΩ
R_2	15 kΩ	20 kΩ
R_3	15 kΩ	20 kΩ
R_4	15 kΩ	20 kΩ
R_a	10 kΩ	10 kΩ
R_b	10 kΩ	10 kΩ
C_1	20 pF	16 pF
C_2	20 pF	16 pF
I_b	10 μA	36 μA

Table 2 MOS transistor aspect ratios.

MOS transistor	W/L
M1-4	20 μm/0.5 μm
M5-8, M13	30 μm/2 μm
M9-12, M14-15	10 μm/2 μm

In this simulation, the aspect ratios of MOS transistors are listed in Table 2. Also we have used the parameters obtained from MOSIS 0.5 μm for other device parameters.

5. Conclusions

In this paper, we have proposed versatile DVCC-based three current-mode IAFs. The IAFs use the grounded resistors at all the x-terminals of the DVCCs reducing the parasitic effects. We have demonstrated that the filter circuits enable ILP, IBP and IHP responses by suitable addition of the circuit current outputs. Additionally the circuit parameters ω_0 and Q can be set orthogonally adjusting the circuit passive elements. Furthermore the voltage-mode IAF configurations have been introduced employing the basic current-mode ones.

The achievement example has been given together with simulation results by PSPICE. The simulation responses have been appropriate enough over a wide frequency range.

The non-idealities (i.e. voltage and current tracking errors) of the DVCC affect the circuit performances. The solution for this will be discussed in the future.

References

[1] Fabre, A., Saaid, O., Wiest, F., and Bouchron, C. 1996. "High Frequency Applications Based on a New Current Controlled Conveyor." *IEEE Transactions on Circuits and Systems* 43 (2): 82-91.

[2] Tsukutani, T., Sumi, Y., and Yabuki, N. 2007. "Novel Current-Mode Biquadratic Circuit Using Only Plus Type DO-DVCCs and Grounded Passive Components." *International Journal of Electronics* 94 (12): 1137-46.

[3] Chipipop, B., and Surakampontorn, W. 1999. "Realisation of Current-Mode FTFN-Based Inverse Filter." *Electronics Letters* 35 (9): 690-1.

[4] Wang, H. Y., and Lee, C. T. 1999. "Using Nullors for Realization of Current-Mode FTFN-Based Inverse Filter." *Electronics Letters* 35 (22): 1889-90.

[5] Gupta, S. S., Bhaskar, D. R., Senani, R., and Singh, A. K. 2009. "Inverse Active Filters Employing CFOAs." *Electrical Engineering* 91: 23-6.

[6] Yuce, E., Tokat, S., Minaei, S., and Cicekoglu, O. 2006. "Low-Component-Count Insensitive Current-Mode and Voltage-Mode PID, PI and PD Controllers." *Frequenz* 60 (3-4): 65-9.

Journal of Electrical Engineering 7 (2019) 23-27
doi: 10.17265/2328-2223/2019.01.005

A Second Order Transition in a Neuron Grid

R. Thieberger[1], A. Rabinovitch[1], A. Vainer[1], I. Aviram[1], Y. Biton[1] and D. Braunstein[2]

1. Physics Department, Ben-Gurion University of the Negev, Beer-Sheva 84105, Israel

2. Sami Shamoon College of Engineering, Beer-Sheva 84100, Israel

Abstract: We perform a simple calculation of a classical cellular automata model based on two types of cells (neurons), excitatory and inhibitory ones, randomly distributed in a 2D space. The only varying parameter is the percentage of inhibitory neurons. Even under such simple conditions, we obtain a transition between two states (which we conjecture to be normal and epileptic). The difference between these states are manifested both in the neuronal activity amplitude and in their frequency. The amplitude changes are shown to be similar to those obtained in a tonic-clonic seizure.

Key words: Cellular automata, epilepsy, seizures, neurons.

1. Introduction

Epilepsy is a major brain malfunction inflicting millions of people worldwide. Although being under extensive investigation both theoretically and experimentally for a long period, real understanding of the basic causes of the phenomenon is still missing. Seizure initiation, maintenance and termination are attributed to many operating causes. Examples are the changes in synaptic effectiveness [1], ion concentrations [2], cation conductance [3], glutamate concentration [4], connection of different brain parts [5] and pH [6]. The model which we wish to present in this work is intimately connected to having in the brain two types of neurons: excitatory and inhibitory. The former when activated deliver to the neurons a positive signal while the second type deliver the command “not to”. A receiving neuron counts the number of impinging “orders” from all neurons it is on their receiving end, and decides whether to function according to the difference between the numbers of the two types. If the number of excitatory received information is larger, it becomes operational and vice versa. In the healthy brain the ratio of the number of excitatory to the inhibitory neurons is approximately 4:1 [7]. Most observations indicate that, during an epilepsy seizure, there is a drop in the inhibitory neutrons. In this paper we assume that this is a fact. It seems that the major reason is the reduction of GABA (γ Aminobutyric acid) [4] which effectively reduces inhibition by decreasing the transmission of information out of such neutrons.

There exist some complex dynamical models, e.g. [8, 9], which use the value of the connection between the inhibitory and excitatory neurons as a bifurcation parameter. A different approach for mathematical modelling of epileptic behavior is based on network theory. e.g. [10].

We would like to treat a dynamical model in order to try to understand the global spatiotemporal basic processes appearing in epilepsy. Such understanding cannot be provided by network methods, which disregard the special attribute. Therefore, we chose a model based on cellular automata (CA) built from such two types of cells, which is possibly the simplest model of the brain conditions.

Cellular automata were first studied by Ulam and von Neumann with the particular purpose of modelling biological self-reproduction (see: Von Neumann [11]). Our Cellular Automaton model consists of a regular grid of cells in two dimensions. Each cell can attain just

Corresponding author: R. Thieberger, Ph.D., professor of physics, research fields: statistical physics, computational physics.

three modes (see below). For each cell a set of cells called its "neighborhood" is defined. An initial state at "time = 0" is assigned to each cell. A new generation is created (advancing "t" by one) by changing the state of each cell according to some rule that is determined by the state of the cell and its neighbors. This change is applied to the whole grid simultaneously. There were just few attempts in the literature to use CA for our problem [12]. Our approach is more similar to the classical method.

2. The Model

Our model consists of a two dimensional array of cells (or "neurons"). Each cell can be either excitatory (E) or inhibitory (I). Both neutron types are distributed randomly in the array. The percentage of the I-neurons is a varying parameter. Each cell can reside in one of three modes: ready (D), Refractory (R) and operating (O). We consider as "neighborhood" both the nearest and next nearest cells of a given central cell. At every cycle each neuron changes according to the following two rules: (1) An O-mode changes into an R-mode, an R mode changes, after a prescribed (an input parameter) number of cycles, into a D-mode, (2) All O-cells of a neighborhood of a D-mode neutron are counted and we subtract from the sum of the E-neurons the sum of the I-neurons. If this is a positive number, we change the D-mode into an O-mode. Following a cycle (i.e. going over all neurons) we update the total number of neurons in mode=O and consider this number as the measure of electric signal emerging from the array.

3. Calculations and Results

In our calculations we assume periodic boundary conditions. We checked also the case of Dirichlet boundary conditions and did not find large differences. Our grid consists of 120 × 120 cells ("neurons"). We chose four cycles for the refractory value. The number of cycles was 12,000. For our Fourier analysis of the results we discarded the first 6,000 cycles. For each case we repeated the calculation five times, and took the average result, so as to eliminate the influence of the randomly chosen distribution of inhibitory neurons. These calculations were performed for many different percentages of inhibitory neurons. As was mentioned before, the total number of neurons which are in the state of firing is our measure of the electric signal. We will call this measure: ρ_e. Results are given in Fig. 1a. Here we show ρ_e as a function of the percentage of inhibitory neurons (ρ_i).

To see if our results are robust, we repeated our calculations using a much larger grid: 360×360 (i.e. Nine times as many neurons). In Fig. 1b we show the results, which do not differ much.

Viewing both of these figures we see that around $\rho_i = 0.2$ we have a change in the slope of the line. We wish to examine this result. For this purpose, we calculate the Fourier transform for different percentage of inhibitory neurons. At $\rho_i = 0.17$ we obtain a peak frequency at 43.9 (see Fig. 2a) whereas at $\rho_i = 0.23$, the peak jumps to 34.7 (see Fig. 2c).

We make the conjecture that this is a transition between a normal state and an epileptic state. As a justification we mention that it is this ρ_i that the normal state goes over to the epileptic state in a real system.

We show next the results of considering a normal state which goes over to an epileptic state and returns after some time back to the normal one. We assume that when the percentage of inhibitory neurons is 19 percent we are in the epileptic state, and when there is 23 percent of inhibitory neurons we are in the normal state. So we calculate ρ_e vs. time when going from $\rho_i = 0.23$ to $\rho_i = 0.19$ and back. To improve our figure, we added another feature. We assume that during the epileptic state we have a certain amount of oscillations in the O-neurons (see [13]). The amount we took in our figure was one percent. In Fig. 3a, we compare the electric excitation as a function of time to those obtained by EEG adopted from Ref. [14] (Fig. 3b). It is seen that even such a simple model can repeat the actual seizure behavior.

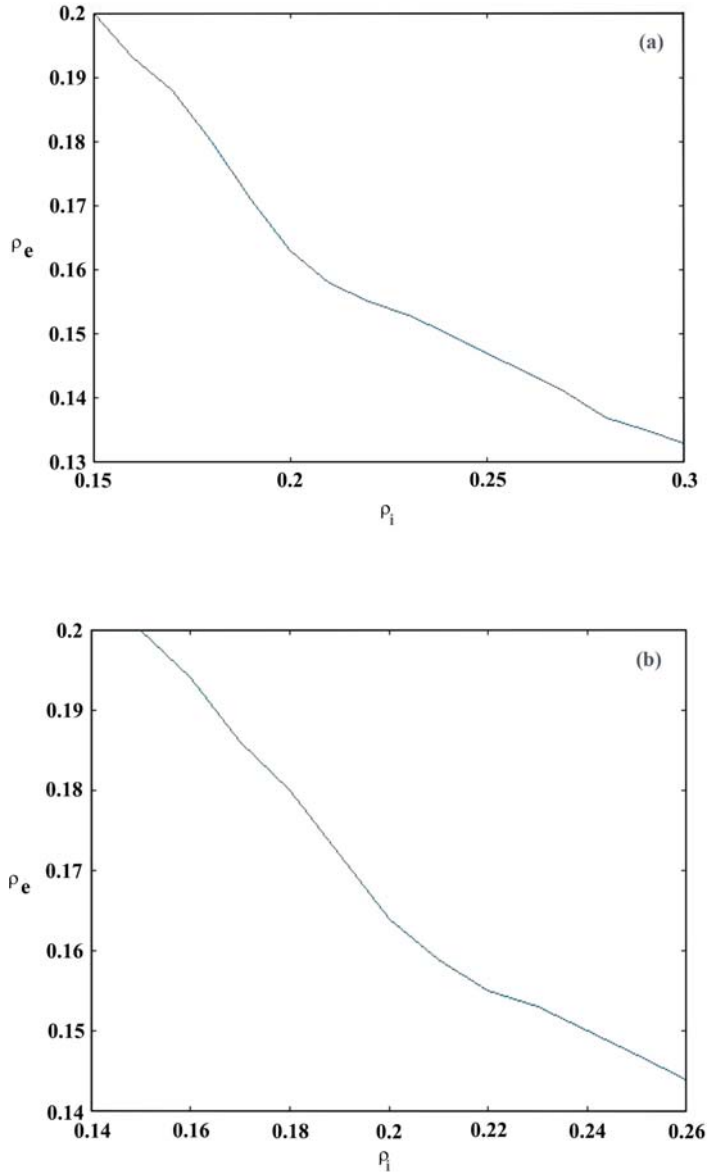

Fig. 1 Relative electric signal as a function of the inhibitory neurons fraction. (a) 120 × 120 grid; (b) 360 × 360 grid.

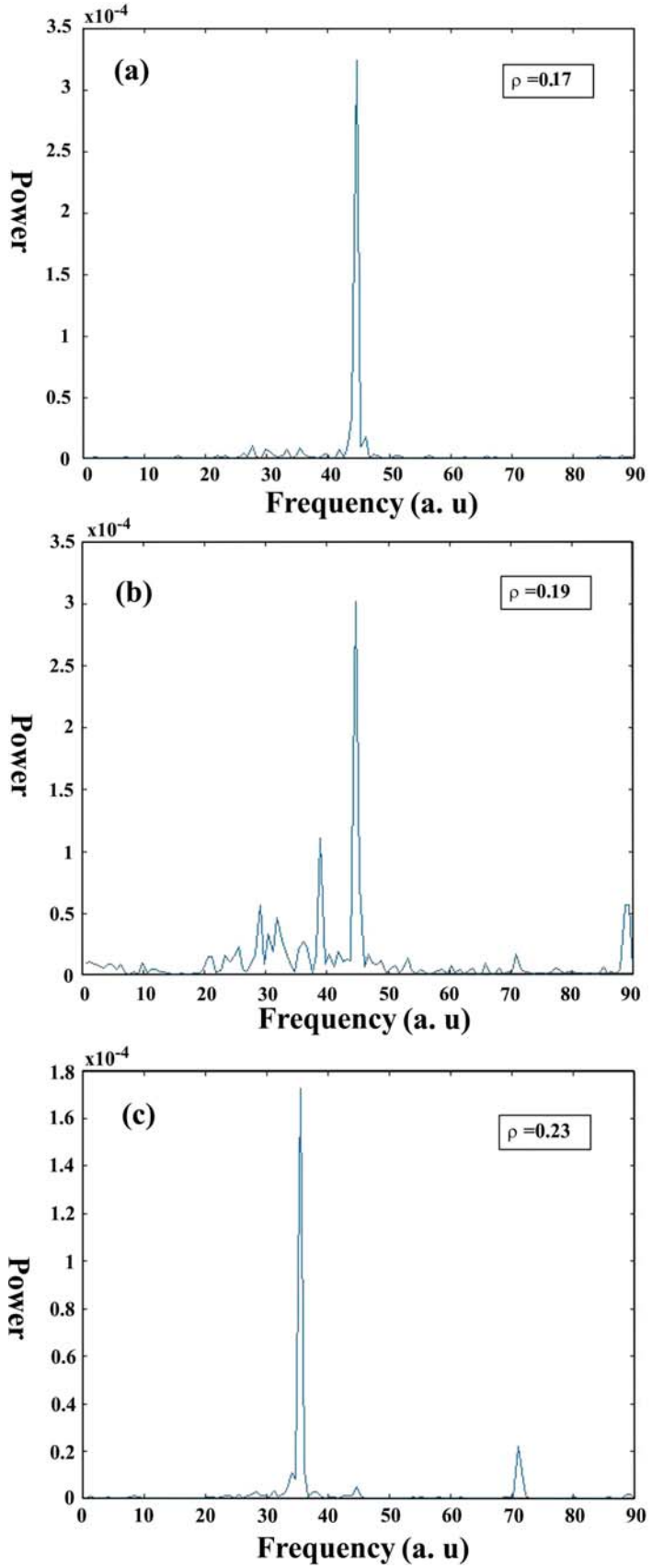

Fig. 2 Fourier power for: (a) 17%, (b) 19% and (c) 23% inhibitory neurons.

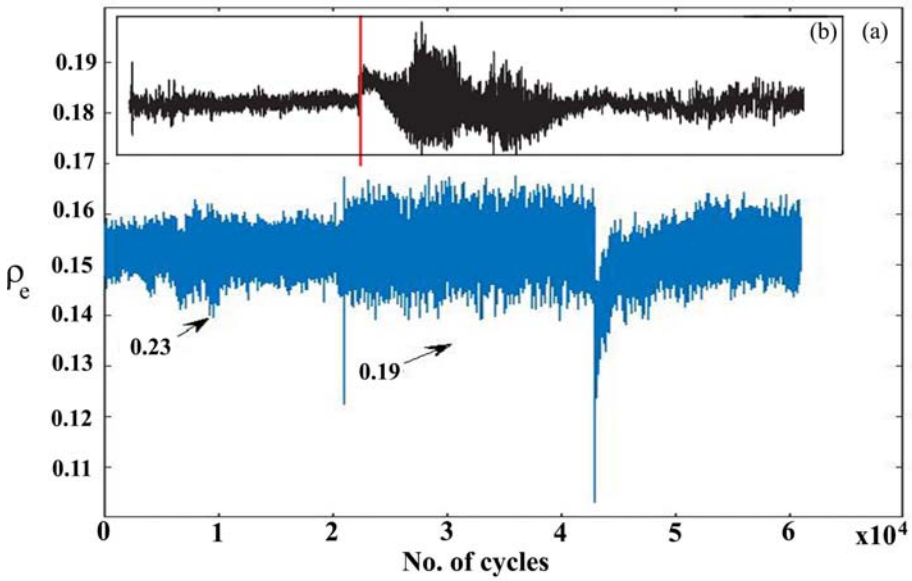

Fig. 3 (a) Relative electric signal for a passage from 23% to 19% and back to 23% of inhibitory neurons; (b) Actual EEG during an epileptic seizure (adapted from Ref. [14]).

References

[1] Froelich, F., Bazhenov, M., Timofeev, I., and Sejnowsky. T. J. 2005. "Mainenance and Termination of Neocortical Oscillations by Dynamic Modulation of Intrinsicand Synaptic Excitability." *Thalamus Relat Syst.* 3: 147-56.

[2] Krishnan, G. P., and Bazhenov, M. 2011. "Ionic Dynamics Mediate Spontaneous Termination of Seizures and Postical Depression State." *J. Neurosci.* 31: 8870-82.

[3] Bal, T., and McKormick, D. A. 1996. "What Stops Synchronized Talamocortical Oscilations?" *Neuron* 17: 297-308.

[4] Kullmann, D. M., and Semyanov. A. 2002. "Glutamatergic Modulation of GABA Signaling among Hipocampal Interneurons. Novel Mechanisms Regulating Hipocampal Excitability." *Epilepsia* 43 (suppl. 5): 174-8.

[5] Norden, A. D., and Blumenfeld, H. 2002. "The Role of Subcortical Structures in Human Epilepsy." *Epil. Behav*. 3: 219-31.

[6] Ziemann, A. E., et al. 2008. "Seizure Termination by Acidosis Depends on ASIC1a." *Nat Neuro-Science* 11: 816-22.

[7] Heiss, J. F., Katz, Y., Ganmor, E., and Lampl, L. 2008. "Shift in the Balance between Excitation and Inhibition during Sensory Adaptation of SI Neurons." *J. Neuroscience* 28: 13320-30.

[8] Cope, D. W., et al. 2009. "Enhanced Uonic GABA Inhibition in Typical Absence Epilepsy." *Nature Medicine* 15: 1392-8.

[9] Hu, C., et al. 2018. "The Generation Mechanism of Spike and Slow Wave Discharges Appearing on Thalamic Delay Nuclei." *Sci Reports* 8: 4953, 1-13.

[10] Jisra, V. K., Stacy, W. C., Quilichim, P. P., Ivanov, A. I., and Bernard, C. 2014. "On the Nature of Seizure Dynamics." *Brain* 137: 2210-30.

[11] Von Neumann, J. 1966. *Theory of Self-reproducing Automata*, edited and completed by Arthur Burks, University of Illinois Press.

[12] Tsoutsouras, V., et al. 2012. "Simulation of Healthy and Epileleptiform Brain Activity Using Cellular Automata." *Journal of Bifurcation and Chaos* 22: 1250229.

[13] Bragin, et al. 1999. "Hipocampal and Entorhinal Cortex High Frequency Oscillations in Human Epileptic Brain." *Epilepsia* 40: 27-37.

[14] McCormick, D. A., and Contreras, D. 2001. "On the Cellular and Network Bases of Epileptic Seizures." *Annu. Rev. Physiol.* 63: 815-46.

Journal of Electrical Engineering 7 (2019) 28-38
doi: 10.17265/2328-2223/2019.01.006

Research and Design of Inverter Applied in Solar PV Systems Connected to Distribution Grid

Nguyen Duc Minh[1], Trinh Trong Chuong[2], Bui Van Huy[2], Quach Duc Cuong[2] and Bui Dinh Thanh[3]

1. Institute of Energy Science, Vietnam Academy of Science and Technology, 18 Hoang Quoc Viet street, Cau Giay district, Hanoi 10072, Vietnam

2. Hanoi University of Industry, No. 298, Cau Dien street, Bac Tu Liem district, Hanoi 11915, Vietnam

3. Hanoi University of Mining and Geology, No.18, Pho Vien, Duc Thang ward, Bac Tu Liem district, Hanoi 11910, Vietnam

Abstract: This paper presents the results of research on the application of inverter in the grid connected solar photovoltaics (PV) system. The main content of the article is to control the three-phase grid connected inverter to meet the requirement of controlling the reactive power to zero at a node of the distribution network while maximizing the active power transmitted to the grid. The control circuits are synthesized on the dq coordinate system and verified on the simulation model by Matlab/Simulink. Both simulation and experimental prototype on 5 kW inverter, being connected to low voltage grid, have been built to show the good results and the practical readiness for implementation.

Key words: SVPWM, reactive power, solar PV, grid connected inverter.

Symbol

Symbol	Unit	Definition
Q	VAr	Measuring and calculation value of reactive power
P	W	Measuring and calculation value of active power
L	H	Inductor
C	F	Capacitor
e_N	V	Alternating power voltage
e_d, e_q	V	Grid voltage on dq coordinates
i_L	A	Current through the coil
i_d, i_q	A	Current through the coil on dq coordinates

1. Introduction

In grid connected solar power systems, the inverter plays an importance role in control systems, as the generated power of solar photovoltaics (PV) system constantly alters due to the weather condition. The alternation of generated power can cause negative impacts on power quality of the grid, such as voltage fluctuation, change in power factor, frequency fluctuation, the increase in the harmonic distortion, etc. The higher and higher demand on the power quality has set out a practical requirement about the necessity of having inverters that can connect flexibly, exchange power and ensure the power quality standards. The aim of the inverter is controlling power among the grid sectors to obtain the most productive capacity of the generator while avoiding sudden conflicts due to loss of transmission or the instability of the generator itself [1]. Apart from the inverter structure, the precision control and stability of electric loop circuit are primary factors in a successful power exchange process.

The main content of this research is to set up control sequences to ensure the control of power factor by 1 and maximize the active power from the solar PV generator to the grid (applied to the non-battery grid connected system). The algorithm and control sequences are systematically analyzed, the research results are proven with the simulated diagram on Matlab and Simulink. They are then verified by a 5 kw experimental model with a PV input that is replaced by a DC source.

Corresponding author: Nguyen Duc Minh, MSc, research fields: electrical system and automatics.

2. Structure of the System and the Controlling Circuit

Fig. 1 presents the diagram of the grid connected solar PV system without backup battery. In this system, DC/DC sets are responsible for executing the power tracking algorithm by the maximum power point tracking (MPPT) algorithm. The DC/AC set must generate a sine-pattern output voltage, ensuring the system's connection (synchronization and monitoring of grids) [2]. The inverter also performs the exchange functions of active power and reactive power between solar PV system and the grid.

2.1 DC/DC Converter

The selected DC/DC converter in the solar PV system is a set of Boost Converter (also known as direct current booster) that is structured as Fig. 2. The controller of the Boost Converter has input voltage given from the solar PV system U_{PV} (Fig. 3). The output of the controller is U_{DC} which processes input for the DC/AC inverter. The MPPT algorithm is involved in this voltage conversion. In this study, the research team used the P&O (Perturb and Observer) MPPT algorithm [3]. This method is simple, popular and easy-to-perform [4].

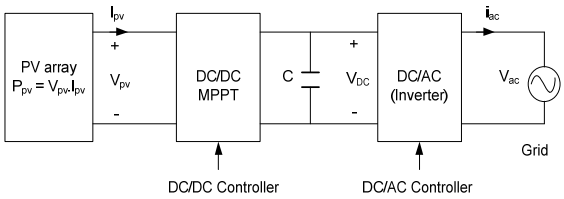

Fig. 1 Principle of grid-connected solar system without battery.

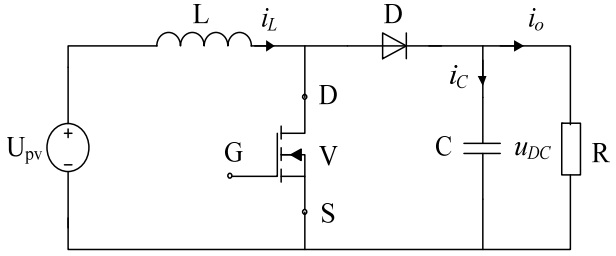

Fig. 2 DC-DC Boost Converter.

This algorithm considers the increase and decrease in voltage periodically to find out the most productive working point. If the variation of voltage makes the power increase, the next variation will remain in the trend of increase or decrease [5]. Conversely, if the variation makes the power decrease, the next variation will change in contrast. When the largest capacity of the working point is defined on the characteristic curve, the voltage variation will fluctuate around the MPPT point (Fig. 4) [6].

The voltage fluctuation causes power loss in the solar PV system [7], especially when the weather conditions change slowly or are stable. This problem can be solved by adjusting logics in P&O algorithm presented in Fig. 5. The P&O algorithm well functions when the weather conditions change dramatically, the maximum power point tracking reaction in a short time and minor adjustments.

The MPPT controller will measure the value of current I and voltage V, then calculate the deviation ΔP, ΔV and check:

- If $\Delta P \cdot \Delta V > 0$, increasing the reference voltage value V_{ref}.
- If $\Delta P \cdot \Delta V < 0$, reducing the reference voltage value V_{ref}.

then replace the previous values with the new V, P value and measure the parameters I, V for the next working cycle. Overall structure of the DC/DC controller system is displayed in Fig. 6.

2.2 DC/AC Inverter

The DC/AC inverter in Fig. 1 is a 3-phase, grid connected inverter. Its circuit structure is presented in Fig. 8, and its function is to convert DC into an AC of 50-60 Hz frequency. When the inverter is applied in a grid connected system, the shortened circuit (one line diagram) of the inverter as Fig. 6 includes converter, R_FC_F filter to minimize the impact of beat rate of current on the voltage frequency of the grid. The inductor L with L_D inductive and R_D resistance is used to balance the voltage difference between the grid and

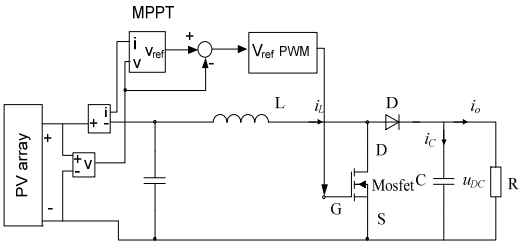

Fig. 3 Principle diagram of Boost Converter controller with MPPT [9].

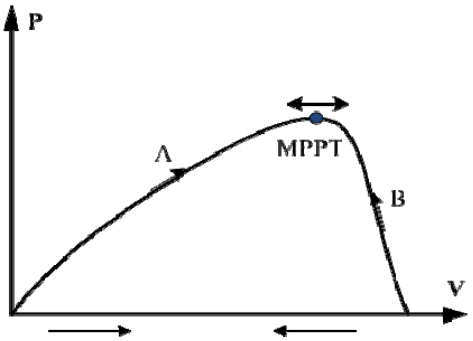

Fig. 4 P&O method to find the largest working power point.

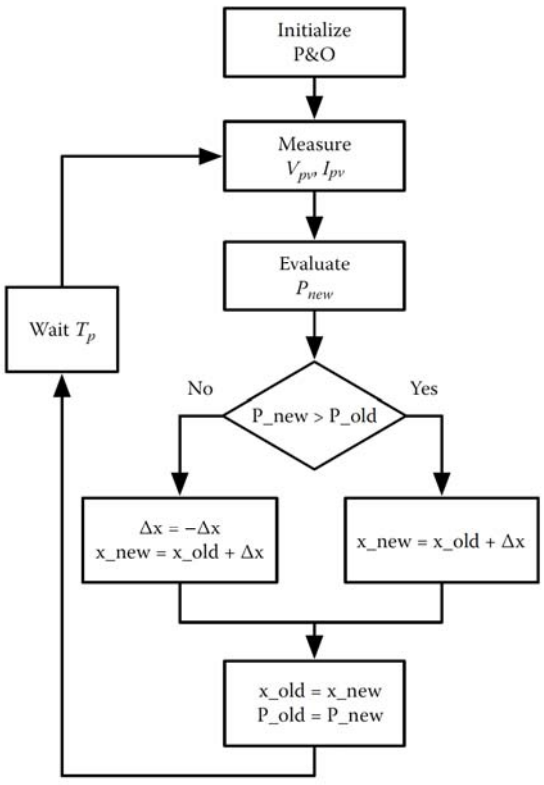

Fig. 5 Steps of conducting P&O method.

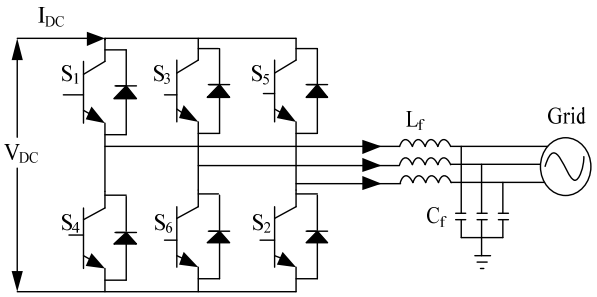

Fig. 6 Structure of three-phase grid-connected inverter.

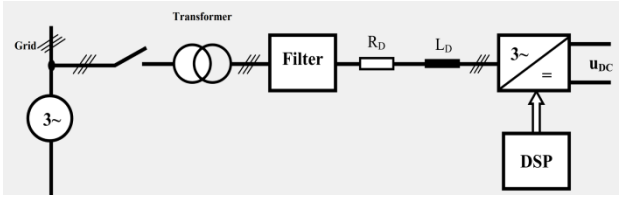

Fig. 7 Principle diagram of grid [8].

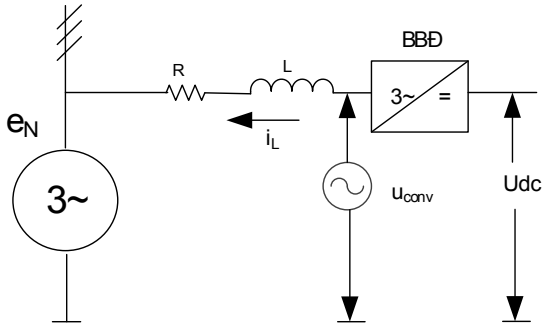

Fig. 8 Alternative diagram of grid circuit.

the output of the converter and to "smooth" the electric current, transformer and circuit breaker. In this study, products with capacity of 5 kW are not too large, so it is possible to omit the capacitors. The principle diagram of the grid connected converter without these steps is shown in Fig. 7.

The circuit including the converter, to filter the chopping impulse voltage, an RC filter, and the inductor L with L_D inductive and R_D resistance are used to filter the current and balance the voltage differences between the grid and the output of the converter, electric current, transformer and circuit breaker. However, it is a system without transformer and filter process. The structure of the grid connected converter is presented as Fig. 8.

When energy transmitted to the grid, the converter functions as an inverter which generates energy from the current circuit to the grid [9]. When the energy transmitted from the grid to the converter, the converter functions as a rectifier, charging energy into the intermediate DC circuit [10]. Applied Kirchhoff law on the alternative diagram:

$$u = Ri_L + L\frac{di}{dt} + e_N \tag{1}$$

Rewrite Eq. (1) on dq coordinates:

$$\begin{cases} \dfrac{di_{Ld}}{dt} = -\dfrac{R}{L}i_{Ld} + \omega i_{Lq} + \dfrac{1}{L}\left(u_d - e_{Nd}\right) \\ \dfrac{di_{Lq}}{dt} = -\dfrac{R}{L}i_{Lq} - \omega i_{Ld} + \dfrac{1}{L}\left(u_q - e_{Nq}\right) \end{cases} \tag{2}$$

Eq. (2) is the status model of the grid inverter system. According to Eq. (2) the controlling unit is the voltage output of the grid inverter, the state vector includes two components i_{Ld}, i_{Lq}.

2.3 Construction of Loop Circuit to Control DC/AC

In terms of control, the two-loop structure consists of an inner loop and an outer loop circuit. The inner loop circuit is the current loop circuit. The outer loop is a power or voltage loop circuit with outstanding advantages. The current loop circuit will help the system to control the current, better respond to the load disturbance, turn off the resonance vibration and protect the overcurrent fault [11]. When the circuit is well designed, the design of the outer loop circuit (voltage, power) also becomes easier. For the external controlled circuit, the goal is to be stable, while in the inner circuit, the requirement is the quick dynamic response capability. Therefore, the authors of the paper proposed a solution of designing a system to control the structure of the two loop circuits as shown in Fig. 9.

2.3.1 Synthesis of Loop Circuit

From Eq. (2), it can be seen that in the loop current equation, there is an interleaving effect between the two axis d and q, and the participation of two grid voltages, called e_d and e_q. The PI controller has the same structure as Eq. (3) to ensure the ability to compensate the channel between the two current components d and q, while also negating the effects of e_d and e_q by the compensatory method:

$$\begin{cases} u_{dref} = \left(K_{p,d} + K_{i,d}\dfrac{1}{s}\right)\Delta I_d + e_d + \omega L i_{Ld} \\ u_{qref} = \left(K_{p,q} + K_{i,q}\dfrac{1}{s}\right)\Delta I_q + e_q + \omega L i_{Ld} \end{cases} \tag{3}$$

in which u_{dref}, u_{qref} are the quantity of output voltage of inverters. The factors of $K_{\text{p,d}}$, $K_{\text{p,q}}$, $K_{\text{i,d}}$, $K_{\text{i,q}}$ are the ratio factors and integral of corresponding adjustment set of axis d and q.

The structure of the inverter controller is shown in Fig. 10. However, due to the current control structure, we have simultaneously offset the channel separation of two components e_d and e_q, in other words the two components e_d and e_q are considered to be disturbance and have been reduced according to the compensatory method; therefore, the obtained system model will consist of two small models on the coordinate axes d, q independently. Ignoring delay due to signal processing delay and sample extracting, the current control structure is shown in Fig. 11.

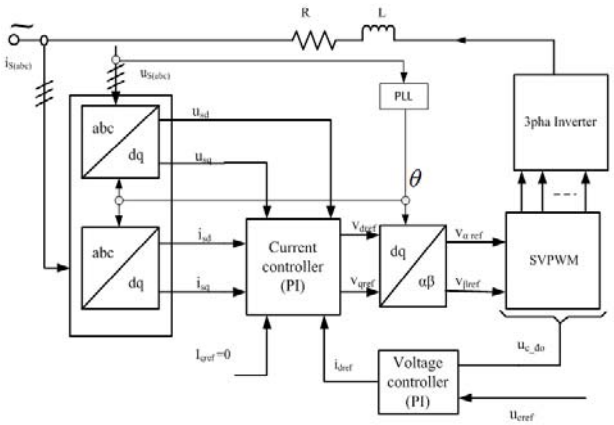

Fig. 9 Structure of grid-connected solar PV controller.

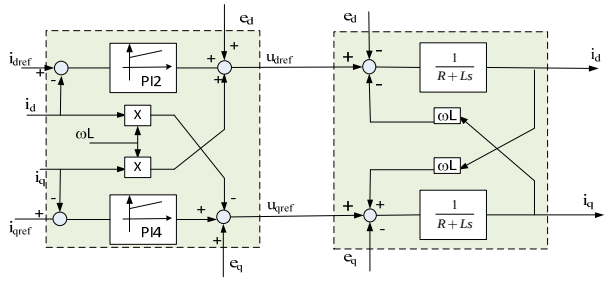

Fig. 10 Structure of controller on dq coordinates.

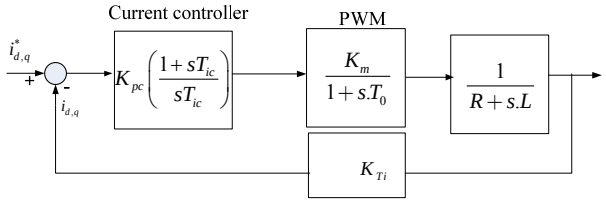

Fig. 11 Block diagram of current controller on dq coordinates.

in which: T_0 is the delay time of the inverter; K_{m} is the amplification factor of the inverter; K_{Ti} is the measuring factor of the power current; K_{pc}, T_{ic} are factors of the controller according to PI law

Transferring function of the open circuit is presented follows:

$$K_{Go} = K_{pc}\left(\frac{1+sT_{ic}}{sT_{ic}}\right)\frac{1}{1+sT_0}\frac{K_0}{1+sT_L} \tag{4}$$

Synthesize the controller according to the optimization method by quantity [4], the factors of the controller are presented in Eq. (5):

$$T_{ic} = T_L = \frac{L}{R};\ \ Kpc = \frac{T_L}{2K_0.T_0} \tag{5}$$

in which:

$$K_0 = K_m.K_L.K_{Ti}; K_L = \frac{1}{R}; T_L = \frac{L}{R}\ \ .$$

Replacing into Eq. (4), the transferring function of the open circuit K_{G0} and that of the close circuit are presented in Eq. (6).

$$\begin{aligned} KG_0 &= \frac{1}{2(1+sT_0)};\\ K_{Gc}(s) &= \frac{I_q(s)}{I_{qref}(s)} = \frac{I_d(s)}{I_{dref}(s)} = \frac{1}{1+s2T_0} \end{aligned} \tag{6}$$

$T_{\mathrm{eq}} = 2T_0$ is the corresponding time constant of the power controlling circuit. It is prioritized by the quantity.

2.3.2 Construction of DC Voltage Controller

The stage of DC power is the intermediate for exchanging energy between power grid and solar PV system. Controlling of DC voltage on the capacitor means controlling the process of active power exchange. The mission of the intermediate DC voltage controller is to stabilize the total DC voltage value on capacitors, outputs of voltage converter are setting value of the current on axis d. Consequently, in order to control the intermediate DC voltage at gate 1, we have to determine the transferring function between the current on axis d and the intermediate DC voltage value U_{dc}. The active power balance equation of DC and AC is presented in Eq. (7).

$$P = \frac{3}{2}\left(e_d i_d + e_q i_q\right) = u_{dc} i_{dc} - P_{loss} = u_{dc} C\frac{du_{dc}}{dt} - P_{loss} \tag{7}$$

in which: u_{C}, i_{C}, P_{loss} is voltage of capacitor, current through the capacitor and power loss of the voltage inverter.

If we ignore the power loss of the voltage inverter and consider the AC power to be symmetric, we have $e_q = 0$, e_d is the amplitude of phase power [10], Eq. (7) will become Eq. (8). Therefore, we have the close loop diagram of the DC voltage converter as in Fig. 12.

$$\frac{du_{dc}}{dt} = \frac{3e_d i_d}{2u_{dc}}\frac{1}{C} \tag{8}$$

In Fig. 13, T_{eq} is the delay time of the current loop circuit; T_f is the delay time of the intermediate DC voltage measuring process on capacitors, K_{Ti} is the current measuring factor. We can simplify the diagram with hypothesis that $T_{\Sigma 2} = T_{eq} + T_f$.

Applying the symmetric priority standard, we can identify the parameters of PI controller as in Eq. (10), with a being the optional parameter.

$$T_{iu} = aT_{\Sigma 2};\ K_{pu} = \frac{2K_{Ti}CU^*_{dc}}{3e_d T_{\Sigma 2}\sqrt{a}} \tag{9}$$

According to Refs. [1, 6, 8]: in order to control Q, we need to control current I_{q}. In case of grid-connected PV, in order to obtain the highest power

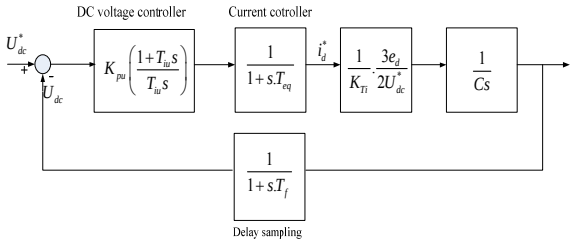

Fig. 12 Block diagram of intermediate DC voltage controller loop.

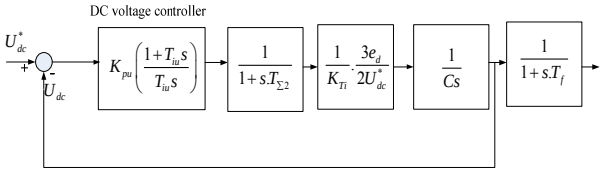

Fig. 13 Equivalent diagram of intermediate DC voltage controller loop.

factor, we select the setting value $i_{qref} = 0$, thereafter, according to Ref. [1], reactive power of the inverter will be 0.

2.4 Principle to Modulate the Space Vector for Inverter (SVPWM)

As presented in Fig. 14, output of loop circuit controlling the current, requires the converting stages of the coordinate from dq/αβ to put into the stage of space vector modulation (SVPWM). The algorithm to modulate the space vector for the 3-phase inverter is presented in Refs. [2, 5]. SVPWM is completely digitalized. The algorithm is simple, easy to apply on the microchips. The algorithm of space vector modulation needs to ensure the output voltage VSI being corresponding to the desired input. The setting value is the desired output voltage, which can be presented in form of polar coordinates $u = U_0.e^{j\theta}$, or perpendicular coordinates u = (u_α, u_β) as in Fig. 15. Vectors $u_{0,1,2,3,4,5,6,7}$ are standard vector, corresponding to the open and close status of valves.

Followings are steps to apply the algorithm to modulate the space vector [2]:

Step 1: Identify the sector of output vector, among 6 sectors presented in Fig. 14. This can be applied in Table 1 and algorithm flowchart in Fig. 15 with $u_\beta^* = u_\beta/\sqrt{3}$.

Step 2: The voltage vector will be synthesized from 2 standard vectors in each sector, therefore, we need to determine the time for executing these 2 standard vectors in the modulation cycle; the inverting circuit status will be zero vector for the remaining time. Fig. 14 presents the voltage vector which is synthesized from 2 standard vectors of u_1 and u_2. The algebraic method is used to determine the modulation factor for voltage vector from two most updated standard vectors in each sector (the modulation factor is the ratio between execution time of standard vectors in each modulation cycle).

As the length of status vector is standardized, with $U_i = (2/3)U_{DC}$, the vectors are presented in the following cordinate, take $\mathbf{u_1}$, $\mathbf{u_2}$ as examples:

$$\mathbf{u}_1 = U_i\left[1,0\right];\mathbf{u}_2 = U_i\left[\frac{1}{2},\frac{\sqrt{3}}{2}\right] \qquad (10)$$

The systhesis of vector $\mathbf{u}$ through $\mathbf{u_1}$, $\mathbf{u_2}$ gives out the following equation:

$$\mathbf{u} = d_1\mathbf{u}_n + d_2\mathbf{u}_m \qquad (11)$$

$\mathbf{u}_n, \mathbf{u}_m$ are two standard vectors in each sector. Factors of d_1, d_2 are calculated according to Eq. (11) and Table 2. For the remaining time, the zero vector will be executed, with the modulation factor of $d_0 = 1 - d_1 - d_2$.

Step 3: The next step is from the modulation factor to execute the standard vectors, it is necessary to determine the modulation factor for each semiconducting valve of the inverter circuit. In order to determine the modulation factor of each semiconducting valve, it is necessary to construct the pulse sample for each sector. This pulse sample is introduced in order to ensure the smallest number of switching of the semiconductor valves in inverter circuit.

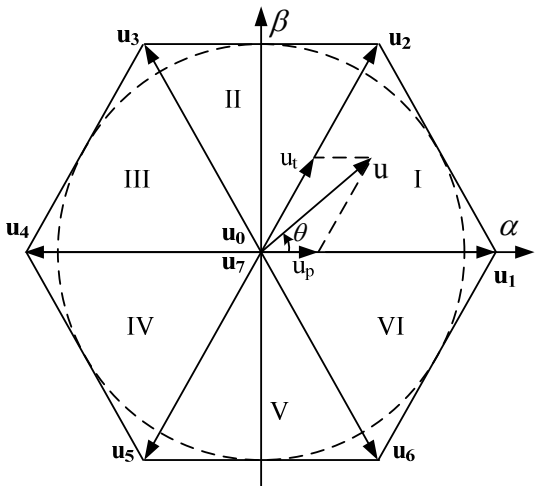

Fig. 14 Space vector, status vectors and sectors.

Table 1 Inequation to determine the position of *u* in sector [2].

	Sector I	Sector II	Sector III
$u_\beta \geq 0$	$u_\beta \geq 0$ $u_\beta < \sqrt{3}u_\alpha$	$u_\beta \geq \sqrt{3}u_\alpha$ $u_\beta > -\sqrt{3}u_\alpha$	$u_\beta \geq 0$ $u_\beta < -\sqrt{3}u_\alpha$
	Sector IV	Sector V	Sector VI
$u_\beta < 0$	$u_\beta < 0$ $u_\beta \geq \sqrt{3}u_\alpha$	$u_\beta < \sqrt{3}u_\alpha$ $u_\beta \leq -\sqrt{3}u_\alpha$	$u_\beta < 0$ $u_\beta \geq -\sqrt{3}u_\alpha$

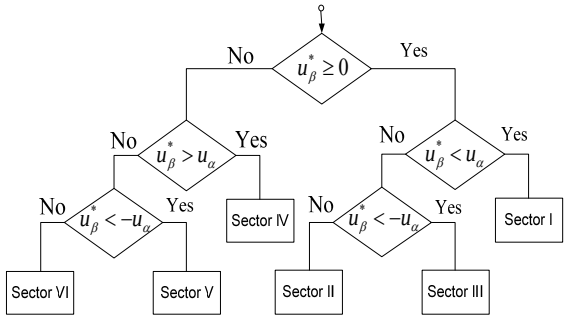

Fig. 15 Algorithm diagram to determine sectors.

Table 2 Matrix synthesis in each sector.

Sector 1 $\mathbf{A}_{nm} = \frac{1}{U_{dc}}\begin{pmatrix} \frac{3}{2} & -\frac{\sqrt{3}}{2} \\ 0 & \sqrt{3} \end{pmatrix}$	Sector 2 $\mathbf{A}_{nm} = \frac{1}{U_{dc}}\begin{pmatrix} -\frac{3}{2} & \frac{\sqrt{3}}{2} \\ \frac{3}{2} & \frac{\sqrt{3}}{2} \end{pmatrix}$
Sector 3 $\mathbf{A}_{nm} = \frac{1}{U_{dc}}\begin{pmatrix} 0 & \sqrt{3} \\ -\frac{3}{2} & -\frac{\sqrt{3}}{2} \end{pmatrix}$	Sector 4 $\mathbf{A}_{nm} = \frac{1}{U_{dc}}\begin{pmatrix} 0 & -\sqrt{3} \\ -\frac{3}{2} & \frac{\sqrt{3}}{2} \end{pmatrix}$
Sector 5 $\mathbf{A}_{nm} = \frac{1}{U_{dc}}\begin{pmatrix} -\frac{3}{2} & -\frac{\sqrt{3}}{2} \\ \frac{3}{2} & -\frac{\sqrt{3}}{2} \end{pmatrix}$	Sector 6 $\mathbf{A}_{nm} = \frac{1}{U_{dc}}\begin{pmatrix} \frac{3}{2} & \frac{\sqrt{3}}{2} \\ 0 & -\sqrt{3} \end{pmatrix}$

$$\begin{bmatrix} d_1 \\ d_2 \end{bmatrix} = \frac{1}{U_{dc}}\begin{pmatrix} \frac{2}{3} & \frac{1}{3} \\ 0 & \frac{1}{\sqrt{3}} \end{pmatrix}^{-1}\begin{bmatrix} u_{S\alpha} \\ u_{S\beta} \end{bmatrix} = \frac{1}{U_{dc}}\begin{pmatrix} \frac{3}{2} & \frac{\sqrt{3}}{2} \\ 0 & \sqrt{3} \end{pmatrix}\begin{bmatrix} u_{S\alpha} \\ u_{S\beta} \end{bmatrix} = \mathbf{A}_{nm}\begin{bmatrix} u_{S\alpha} \\ u_{S\beta} \end{bmatrix} \quad (12)$$

3. Modelling and Experiment

3.1 System Modelling

The simulation diagram of the controlling system of the inverter using Matlab/Simulink software is presented in Fig. 16, in which the VSC Control is the stage of executing the controlling algorithm of the 3-phase voltage inverter. The configuration of the controller is presented in Table 3 [11].

Boost Converter, or so-called DC-DC voltage converter, gives out the output voltage which is larger than the input voltage (simulation diagram in Fig. 17). The basic circuit contains 2 switching semiconductors (one diode and one transistor) and a coil L, a capacitor C, load R. The MPPT controller uses the algorithm with maximum capacity P&O as presented above.

The analysis results of the model, presented in Fig. 18, show that when the solar radiation is about 1,050 (W/m^2), the power *P* generated to the grid is 5 kW. The output voltage of the DC/DC converter is the setting value of the intermediate DC voltage controller U_{DC}. The simulation results of Fig. 19 show that the intermediate DC voltage is stable when the system is at identified status, which means the power exchange process is balanced.

The power quality generated to the grid is good, with the analysis results of current pattern and 4-phase harmonization wave at two presentative points of time t = 2 s as presented in Fig. 20. The simulation results

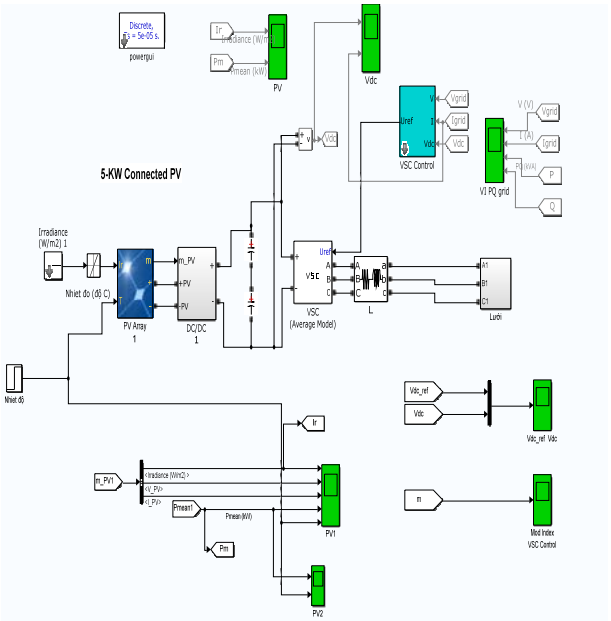

Fig. 16 Simulation diagram of grid-connected solar PV system.

Table 3 Configuration of the controller.

Controller	K_p	K_i
DC voltage controller	20	100
Current controller (dq)	0.015	1

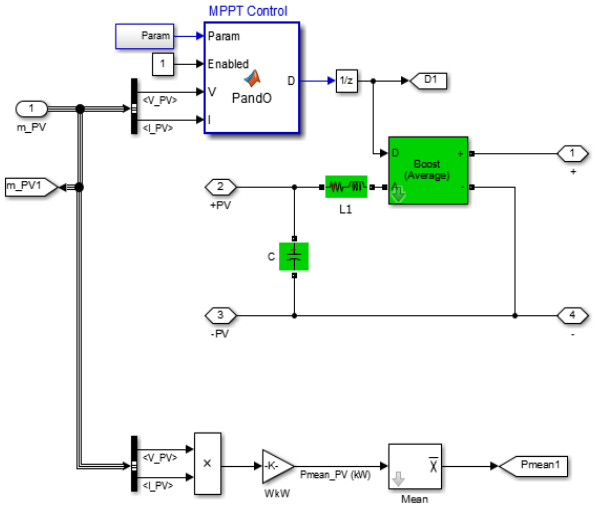

Fig. 17 Explanation diagram of DC/DC.

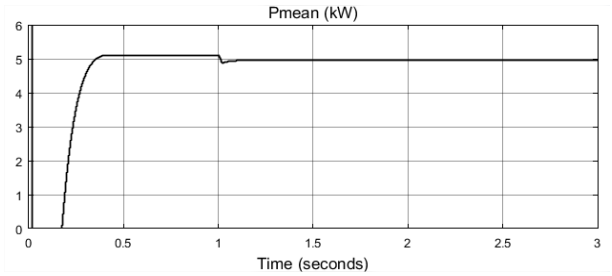

Fig. 18 Active power from PMT to converter.

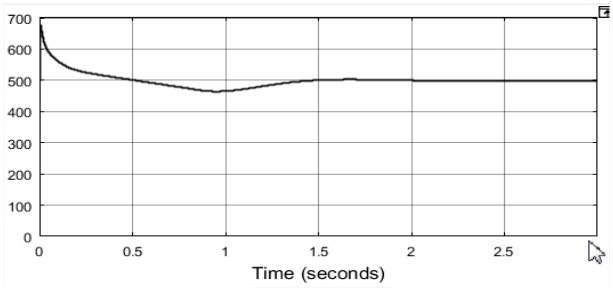

Fig. 19 DC power on capacitor.

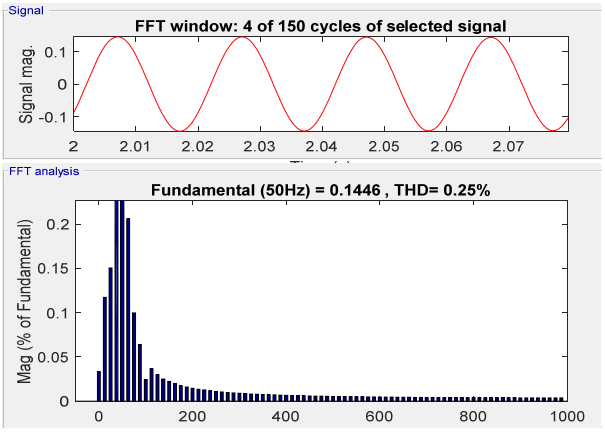

Fig. 20 Analysis of harmonization wave in form of power into the grid at t = 2 s.

of power P, Q in Fig. 21 show that power Q is controlled to 0 in very short time, at around 0.7 s, which ensures the power factor of the current generated to the grid is the highest. The active power generated to the grid is nearly 4.5 kW, compared to the capacity of solar battery generated to the inverter which is 5 kW. The efficiency is about 90%.

3.2 Experiment Results

In order to verify the space vector modulation algorithm for grid-connected three-phase set, we constructed the experimental system. The comprehensive system is presented in Fig. 22. Component modules of the system have been designed and manufactured successfully, as presented in Figs. 23-25. The analysis results of measuring wave patterns into IGBT valves, intermediate DC voltage and analysis results of the harmonization wave are presented in Figs. 26-28.

3.2.1 Efficiency Experiment

We conduct 3 experiment with different loads.

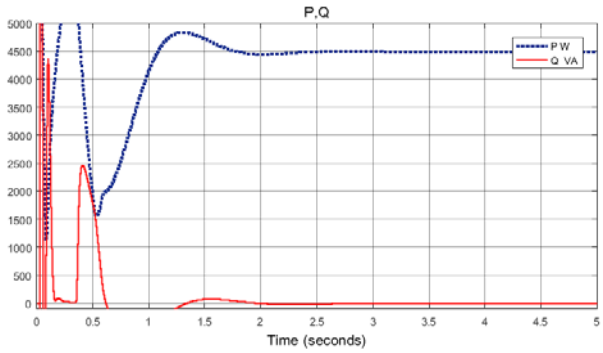

Fig. 21 Active power (dot line) and reactive power (solid line) into the grid.

Fig. 22 Comprehensive equipment.

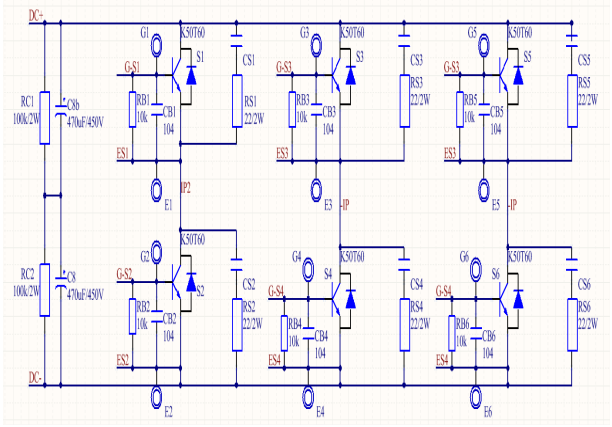

Fig. 23 Diagram of three-phase inverter force circuit.

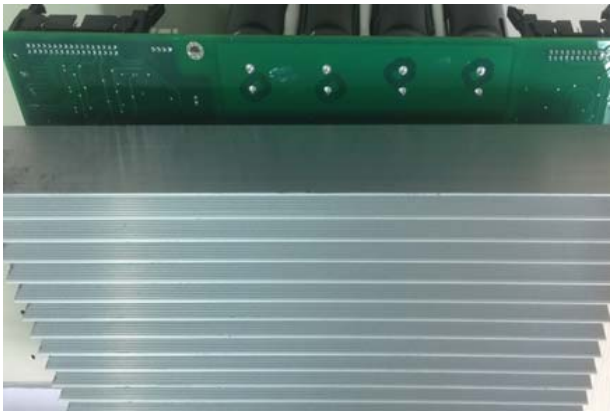

Fig. 24 Block of force circuit with heat radiator.

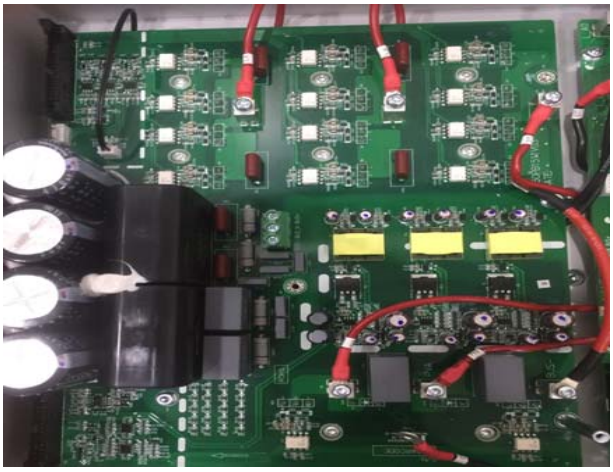

Fig. 25 DC capacitor module and connected block.

1st time: 25 florescent light bulbs 60 W + 8 fans 72 W

- DC input voltage: U_{DCt} = 220 V
- DC input current: I_{iDC} = 9.4 A
- AC output power: P_{AC} = 1,822.33 W

Converting efficiency (%): P_{AC}/P_{DC} = 1,822.33 / (220 × 9.4) × 100% = 88.12%

2nd time: 3 air conditioning systems 9,000 BTU (equivalent to 2,238 kW)

- DC input voltage: U_{DCt} = 220 V
- DC input current: I_{iDC} = 10.17 A
- AC output power: P_{AC} = 2,001.1 W

Converting efficiency (%) P_{AC}/P_{DC} = 2,001.1 / (220 × 10.17) × 100% = 89.43%

3rd time: 3 air conditioning systems 12,000 BTU (equivalent to 2,984 kW)

- DC input voltage: U_{DCt} = 220 V
- DC input current: I_{iDC} = 13.6 A
- AC output power: P_{AC} = 2,690.4 W

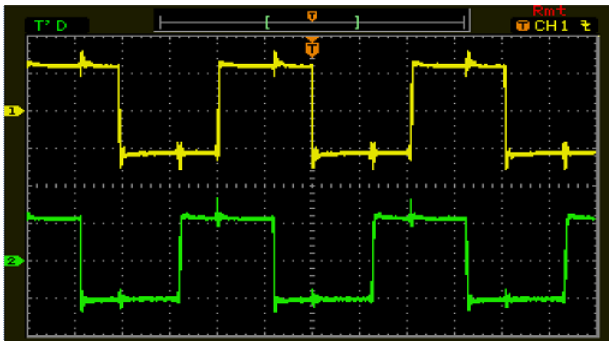

Fig. 26 Measuring wave pattern into the IGBT valve DC-DC and DC-AC modules.

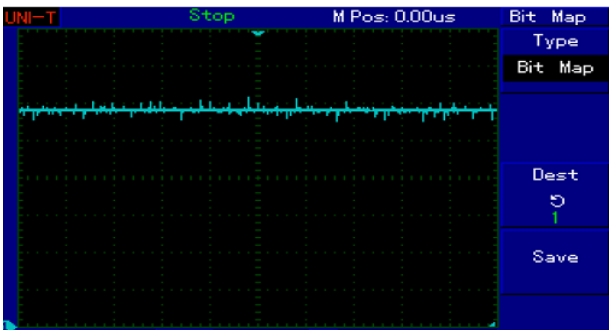

Fig. 27 Intermediate DC power pattern.

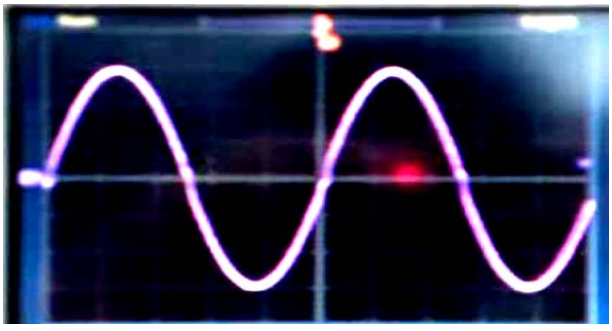

Fig. 28 One-phase power pattern to the grid.

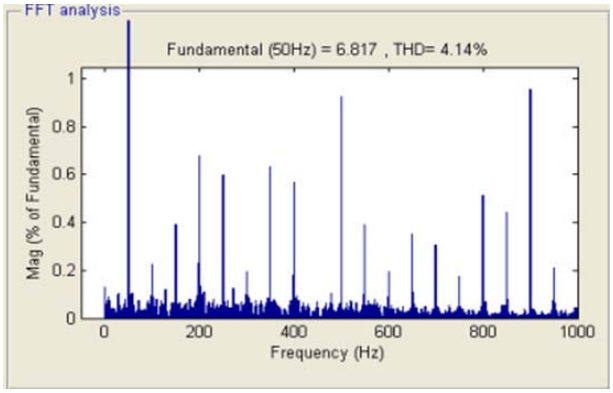

Fig. 29 Analysis results of harmonization wave.

Converting efficiency (%) P_{AC}/P_{DC} = 2,690.4 / (220 × 13.1) × 100% = 89.9%.

Conclusion on converting efficiency after three times of measuring, the average result is 89.15%.

3.2.2 Testing on Harmonization Waves

In line with efficiency evaluation we also measure the harmonization wave spectrum using digital oscilloscope as presented in Fig. 29, the results show that the harmonic distortion is 4.14% (< 5%).

In addition, we also conduct with pure resistant load and inductive load with different capacities, the results show that:

• Output frequency f = 50 Hz with error of ± 0.1 Hz. AC output voltage with effective value meets the requirement, the sin output wave pattern with harmonization component is acceptable.

• The output power meets the requirement of design, when being tested on different loads. The average converting efficiency is 89.15%.

• The DC input voltage from the working solar panel ranges from 16 V to 36 V, which can be expanded to 45 V_{DC}.

4. Conclusion

The article has built a control system for the converter. The DC current and intermediate voltage control loops are analyzed and designed. The paper builds simulation models of input voltage inverter with full physical and systematic significance, based on sufficient assumptions.

Simulation results show that the inverters used in grid-connected solar systems have worked well. The results are convincing and practical. The experimental results on the actual model show good results, proving the proposed solution.

Equipment efficiency will be improved in the near future by raising the hash frequency and selecting highly efficient accessories.

Acknowledgements

This paper is developed as a component of the study "Research, Design and Manufacture of Highly Efficient Inverter Connected to Distribution Grid for Solar PV System" Code: VAST07.04/18-19. The authors specially thank the Vietnam Academy of Science and Technology, Institute of Energy Science for providing fund for the study.

References

[1] Sanchez, C. A. 2010. "Control Design for Electronic Power Converters." Ph.D. thesis, Institut National Polytechnique de Grenoble; Universidad de Sevilla.

[2] Erickson, R. W., and Maksimovic, D. 2001. *Fundamentals of Power Electronics*. New York: Kluwer.

[3] Freeman, D. 2010. *Introduction to Photovoltaic Systems Maximum Power Point Tracking*. Texas Intruments, Application report.

[4] Hwang, J. W. G., Winkelnkemper, M., and Lehn, P. W. 2006. "Design of an Optimal Stationary Frame Controller for Grid Connected AC-DC Converters. IEEE Industrial Electronics." Presented at the IECON 2006- 32nd Annual Conference on IEEE Industrial Electronics, Paris, France.

[5] Quang, N. P., and Dittrich, J. 2008. *Vector Control of Three-Phase AC Machine: System Development in the Practice*. Heidelberg: Springer.

[6] Augustine, S., Lakshminarasamma, N., and Mishra, M. K. 2016. "Control of Photovoltaic-Based Low-Voltage DC Micro Grid System for Power Sharing with Modified Droop Algorithm." *IET Power Electron.* 9 (6): 1132-43.

[7] Kazmierkowski, M. P., Krishnan, R., and Blaabjerg, F. 2012. *Control in Power Electronics*. Elsevier Science.

[8] Senjyu, T., Miyazato, Y., Yona, A., and Urasaki, N. 2008. "Optimal Distribution Voltage Control and Coordination with Distributed Generation." *IEEE Trans. Power Deliv.* 23: 1236-42.

[9] Ibrahim, H. E. A., and Ibrahim, M. 2012. "Comparison Between Fuzzy and P&O Control for MPPT for

Photovoltaic System Using Boost Converter." *Journal of Energy Technologies and Policy* 2 (6).

[10] Amirnaser, Y., and Reza, I. 2010. *Voltage-Sourced Converters in Power Systems.* Wiley-IEEE Press. ISBN: 978-0-470-52156-4.

[11] Bui, V. H., Chan, T. M., and Nguyen, V. L. 2014. "Controlling AC Power through Multi-step AC-DC-AC-AC Converter with High Frequency Intermediate Stage." *Technical Journal of Control and Automation, December*. (in Vietnamese)

Journal of Electrical Engineering

Volume 7, Number 1, Jan.-Feb. 2019

David Publishing Company

616 Corporate Way, Suite 2-4876, Valley Cottage, NY 10989, USA

Tel: 1-323-984-7526, 323-410-1082; Fax: 1-323-984-7374, 323-908-0457

http://www.davidpublisher.com, www.davidpublisher.org

electrical@davidpublishing.com, electrical@davidpublishing.org